https://doi.org/10.5194/egusphere-2026-1666
Preprint. Discussion started: 27 May 2026

Beyond aerosol size parameter comparison: A practical method for evaluating aerosol microphysical processes of 3D aerosol physics and chemistry models using size-resolved aerosol measurement data−Application to NHM-Chem v2.0

Mizuo Kajino[1,2], Narihiro Orikasa[1], Rei Kudo[1], Atsushi Shimizu[3], Tomoaki Nishizawa[3], Yoshitaka Jin[3], Kazuo Osada[4], Satoko Kayaba[3], Tomoki Kajikawa[5,1], Rio Ishikawa[5,1], and Keiya Yumimoto[6]

[1]Meteorological Research Institute (MRI), Japan Meteorological Agency (JMA), Tsukuba, Ibaraki 305-0052, Japan
[2]Faculty of Life and Environmental Sciences, University of Tsukuba, Tsukuba, Ibaraki 305-8572, Japan
[3]National Institute for Environmental Studies (NIES), Tsukuba, Ibaraki 305-8506, Japan
[4]Graduate School of Environmental Studies, Nagoya University, Nagoya, Aichi 464-8601, Japan
[5]Graduate School of Science and Technology, University of Tsukuba, Tsukuba, Ibaraki 305-8572, Japan
[6]Research Institute for Applied Mechanics, Kyushu University, Kasuga, Fukuoka 816-8580, Japan

Correspondence to: M. Kajino (kajino@mri-jma.go.jp)

Abstract. Aerosol size is a key parameter for evaluating the climate and environmental impacts of aerosols. However, when discrepancies arise between simulated and observed aerosol size-distribution parameters (e.g., number concentration, mean diameter, and standard deviation), it is often difficult to judge how critical those differences are. Here, we propose a practical recipe for evaluating 3-D aerosol models with size-resolved measurement data: the Pseudo-physical Variable Comparison (PPVC) method. PPVC compares physically meaningful variables (e.g., cloud condensation nuclei concentrations and light extinction coefficients) and processes (e.g., condensation rate and Brownian coagulation rate) that are derived from observed and simulated size distributions of aerosols, together with prescribed representative values of relevant parameters (e.g., hygroscopicity or refractive index), instead of comparing only size parameters. We applied PPVC to evaluate a regional-scale meteorology–chemistry model, NHM-Chem (versions v1.0 and v2.0), using scanning mobility particle sizer (SMPS) and aerodynamic particle sizer (APS) data measured in Tsukuba. The PPVC analysis showed that v2.0 improved the predictability of light extinction coefficients relative to v1.0. Using independent datasets, we also found that NHM-Chem v2.0 generally outperformed v1.0 not only for aerosol optical depth (AOD) but also for the predicted fine-mode fractions of inorganic species, owing to improvements in aerosol size distributions. We propose a new metric to evaluate the overall consistency of simulated aerosol physical parameters: the Distance of Deviations between simulated and observed Aerosol Physical Parameters (DD_{AP}). DD_{AP} for NHM-Chem v1.0 and v2.0 were 4.2×10^{-2} and 3.5×10^{-2}, respectively, indicating that the microphysical properties and processes simulated by v2.0 were approximately 17% more consistent with observations than those of v1.0.

https://doi.org/10.5194/egusphere-2026-1666
Preprint. Discussion started: 27 May 2026

1 Introduction

Aerosol size is a key parameter for assessing the climate and environmental impacts of aerosols. Aerosols influence the climate through aerosol–radiation–cloud interaction processes (e.g., Szopa et al., 2021), and they affect the environment after deposition to the ground (e.g., Burns et al., 2011) or into the respiratory tract (e.g., Cohen et al., 2004). The importance of aerosols varies substantially with particle size, which spans roughly from 1 nm to several 10 μm in diameter. Particles smaller than several 10 nm generally have negligible influences on climate because they do not efficiently interact with solar radiation and are not activated as cloud condensation nuclei (CCN). However, because the number concentrations of such tiny particles can be very large, they may substantially influence the climate once they grow by condensation or heterogeneous chemistry to larger sizes. Most aerosol mass is associated with particles larger than ~100 nm, namely submicron (fine mode, several 100 nm) and supermicron (coarse mode, several μm) particles; these size modes therefore strongly influence environmental and climatic impacts. Removal processes depend strongly on size. Brownian motion and gravitational settling are slow for submicron and coarse-mode particles, so these particles are not readily removed by dry deposition, below-cloud scavenging, or respiration unless their diameters exceed several micrometers and their inertia becomes large. Removal rates of submicron and coarse-mode particles vary by orders of magnitude with size (e.g., Greenfield, 1957; Petroff and Zhang, 2010; Wang et al., 2010; Zhang et al., 2013).

Accurate prediction of aerosol size distributions is therefore indispensable for realistic simulations of climate and environmental impacts. Observed atmospheric aerosol size distributions are often well approximated by combinations of lognormal modes, so modal aerosol microphysics models that assume lognormal size distributions have been widely used (e.g., Whitby et al., 1991). Sectional (bin) models solve the evolution of aerosol size distributions by discretizing the particle size domain into size bins (e.g., Gelbard et al., 1980). There are other advanced techniques, the particle-resolving approach (Riemer et al., 2009) and the modal bin hybrid model (Kajino et al., 2013a). Modal and sectional aerosol microphysics schemes have been implemented in many 3-D climate and air-quality models. Model evaluation commonly compares the shapes of number size distributions, $n(D)$, or derived parameters such as total number concentration (N), N above x nm (CN_x), geometric mean diameter (D_g), geometric standard deviation (σ_g), or moments (M_k) with observations (e.g., Guelle et al., 2001; Easter et al., 2004; Fast et al., 2006; Spracklen et al., 2007; Elleman and Covert, 2009; Yu and Luo, 2009; Luo and Yu, 2011; Mann et al., 2012; Patoulias et al., 2018; Tagen et al., 2019; Leinonen et al., 2022; Mao et al., 2025) (Fig. 1a).

However, when simulated and observed aerosol size distribution parameters differ, it is often difficult to determine whether a given discrepancy is consequential for 3-D model predictions (Fig. 1b). For example, large differences between N_{sim} and N_{obs} for submicron or coarse-mode particles can materially affect climate and environmental simulations, whereas differences in N for particles (smaller than several 10 nm) may have negligible effects on 3-D simulations. Similarly, the impact of errors in D_g and σ_g depends strongly on the size range. A given percentage error (for example, 20%) in σ_g can have very different consequences in the 3D simulations depending on whether σ_g is small (for example, 1.2 → 1.44) or large (for

https://doi.org/10.5194/egusphere-2026-1666
Preprint. Discussion started: 27 May 2026

example, 2.0 → 2.4). Therefore, there should not exist an absolute standard for how large errors in the aerosol size parameters can be acceptable.

To address this interpretive gap, we propose the Pseudo-Physical Variable Comparison (PPVC) method to quantify model errors in aerosol microphysical variables and processes that directly affect climate and environmental predictions in 3-D simulations. As shown in Fig. 1c, instead of focusing on size parameters, the PPVC method compares observed and simulated pseudo-physical variables (PPVs) that are derived from $n(D)$. Examples of PPVs include the condensation sink of a condensing gas, the coagulation sink for particles of a given size, the CCN number concentration at a given supersaturation, and the light extinction coefficient at a given wavelength. These PPVs are calculated by integrating observed $n(D)$ from size-resolved instruments, such as Scanning Mobility Particle Sizer (SMPS) and Aerodynamic Particle Sizer (APS), and simulated $n(D)$ discretized into SMPS and APS bins, together with prescribed common physical parameters that are typically observed or assumed in the atmosphere (Fig. 1c).

In Sect. 2, we present the simulation settings and the observational datasets used for PPVC evaluation (Sects. 2.1 and 2.2), and we describe the derivations of the PPVs in Sect. 2.3. In Sect. 3, we prioritize extinction-to-volume ratio (EVR) among the PPVs to guide model improvement, and we document improvements in EVR from NHM-Chem from v1.0 to v2.0. In Sect. 4, we compare NHM-Chem v1.0 and v2.0 against independent datasets, including lidar observations over Northeast Asia and $PM_{2.5}$ and PM_{10} ion-chromatography measurements at Tottori University. In Sect. 5, we propose and discuss a new metric, the Distance of Deviations between simulated and observed Aerosol Physical parameters (DD_{AP}), and Sect. 6 summarizes major conclusions and future work.

https://doi.org/10.5194/egusphere-2026-1666
Preprint. Discussion started: 27 May 2026

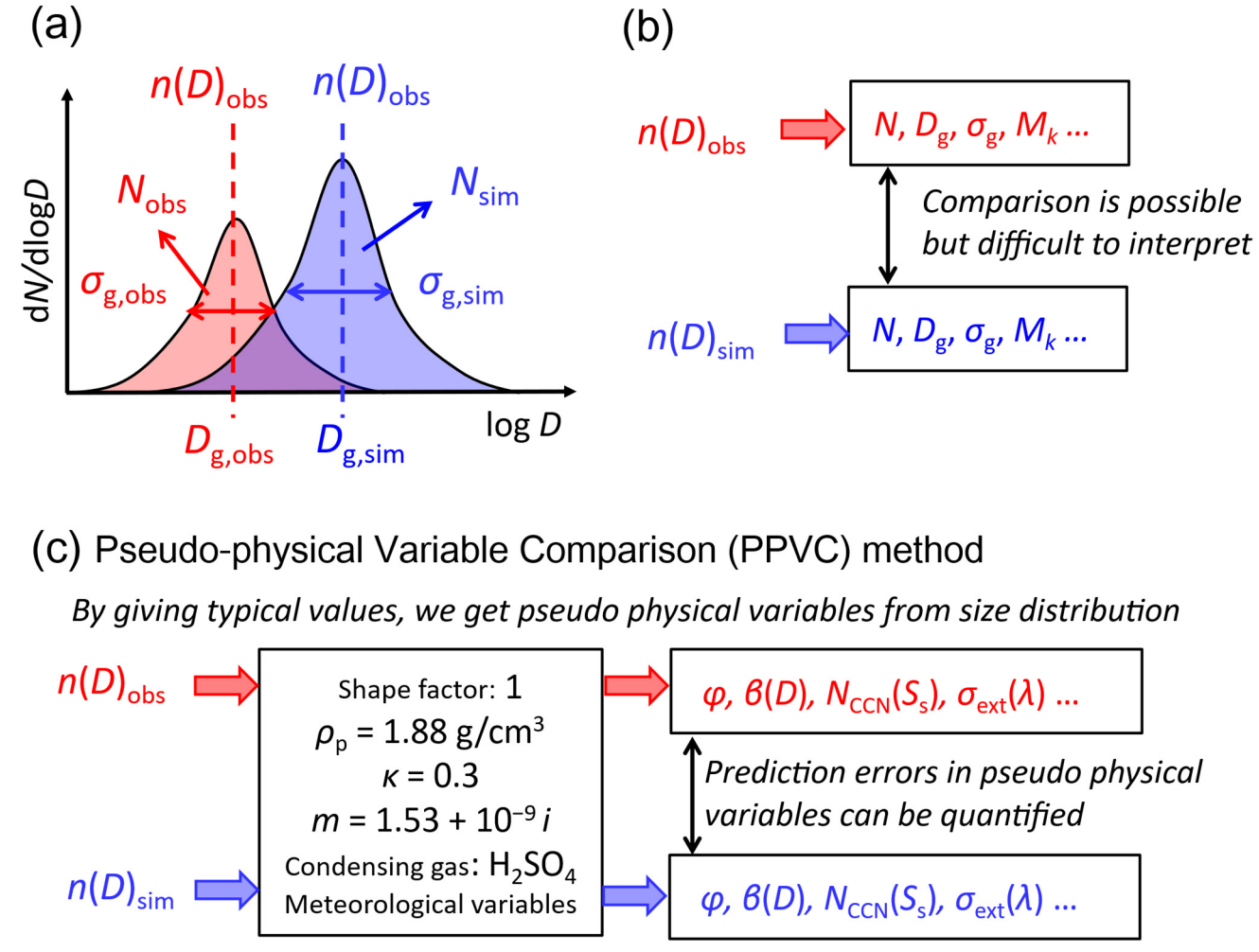

Figure 1: Conceptual illustration describing the PPVC method. (a) Number size distributions of atmospheric aerosols $n(D)$ are well approximated by lognormal distribution functions, which are represented by total number N, geometric mean diameter D_g, and geometric standard deviation σ_g. (b) For the model evaluation, comparisons of observed and simulated aerosol size parameters, such as N, D_g, σ_g, and k-th moment M_k, are feasible, but interpretation is difficult. For example, we do not know whether 20% error in σ_g is really large or not. (c) The PPVC method is proposed to compare observed and simulated PPVs, such as condensational sink of a condensing gas, φ, coagulation sink of a particle with a size of D, $\beta(D)$, number concentrations of CCN at a supersaturation S_s, $N_{CCN}(S_s)$, and light extinction coefficient at a wavelength λ, $\sigma_{ext}(\lambda)$, derived from the observed and simulated $n(D)$ and the prescribed common physical parameters, which are typically observed or assumed in the atmosphere, such as shape factor = 1, particle density ρ_p = 1.88 g cm^{-3}, hygroscopicity κ = 0.3, refractive index $m = 1.53 + 10^{-9}i$ at a wavelength of 532 nm, and condensing gas of H_2SO_4.

https://doi.org/10.5194/egusphere-2026-1666
Preprint. Discussion started: 27 May 2026

2 Methods

2.1 Numerical simulation

2.1.1 Regional meteorology–chemistry model (NHM-Chem)

We used the Japan Meteorological Agency (JMA) regional meteorology–chemistry model, the nonhydrostatic model NHM-Chem (Kajino et al., 2019; 2021). NHM-Chem is a chemical transport model (CTM) that can be run either offline or online coupled to JMA's previous-generation operational numerical weather prediction model, NHM (Saito et al., 2006; 2007). In this study, we developed NHM-Chem v2.0; major updates relative to v1.0 include implementations of online meteorology–chemistry coupling and aerosol–meteorology feedback (Kajino et al., 2026), and improved aerosol size distribution representation. In this study, offline-coupled NHM-Chem was used and tested. We used the five-category non-equilibrium module described by Kajino et al. (2019, 2021), which includes Aitken mode (ATK), soot-free accumulation mode (ACM), accumulation mode internally mixed with soot aggregates (AGR), mineral and anthropogenic dust (DU), and sea salt (SS). NHM-Chem simulates emissions, transport, photochemical gas- and aerosol-phase chemistry, aerosol microphysics, liquid-phase chemistry, and dry, wet, and cloud deposition processes (Kajino et al., 2019; 2021).

Figure 2 shows the model domain covering East Asia. The horizontal grid resolution is 30 km on a Lambert conformal projection, consistent with Kajino et al. (2019, 2021). The domain comprises 200 × 140 horizontal grid points. The NHM employs 38 vertical levels up to 22,055 m mean sea level (m.s.l.), and the CTM uses 40 vertical levels up to 18,000 m m.s.l., both with terrain-following coordinates. The Japanese 55-year Reanalysis (JRA-55; 6-hourly, 1.25° × 1.25°; Kobayashi et al., 2015) provided initial and boundary meteorological conditions. JRA-55 was also used for spectral nudging above 7 km to constrain large-scale wave components (wavelength > 1,000 km) of horizontal momentum and potential temperature; the nudging weighting factor was 0.06 (Nakano et al., 2012). For chemical initial and boundary concentrations, we used monthly climatological fields (11-year mean, 2003–2013) from the Meteorological Research Institute Chemistry–Climate Model version 2 (MRI-CCM2; Deushi and Shibata, 2011) for gaseous species, and the Model of Aerosol Species IN the Global Atmosphere (MASINGAR mk-2; Tanaka and Ogi, 2017) for aerosol species. The anthropogenic emission inventory used was REASv3.2.1 (monthly, 0.25°; Kurokawa and Ohara, 2020), with diurnal profiles for each emission sector from Li et al. (2017). Biogenic emissions came from MEGAN2 (Guenther et al., 2006), and biomass-burning emissions from GFED4 (Giglio et al., 2013). Volcanic SO_2 emissions were prescribed from JMA observation data (Kajino et al., 2021). The simulation period covered one year, from 1 July 2015 to 1 July 2016, with a spin-up of 5 days (the run started on 26 June 2015).

Horizontally, model values were interpolated to observation sites using an inverse-distance-squared weighting of the four nearest grid points. Vertically, the model grid box closest heigt to each observation site was used for comparisons.

https://doi.org/10.5194/egusphere-2026-1666
Preprint. Discussion started: 27 May 2026

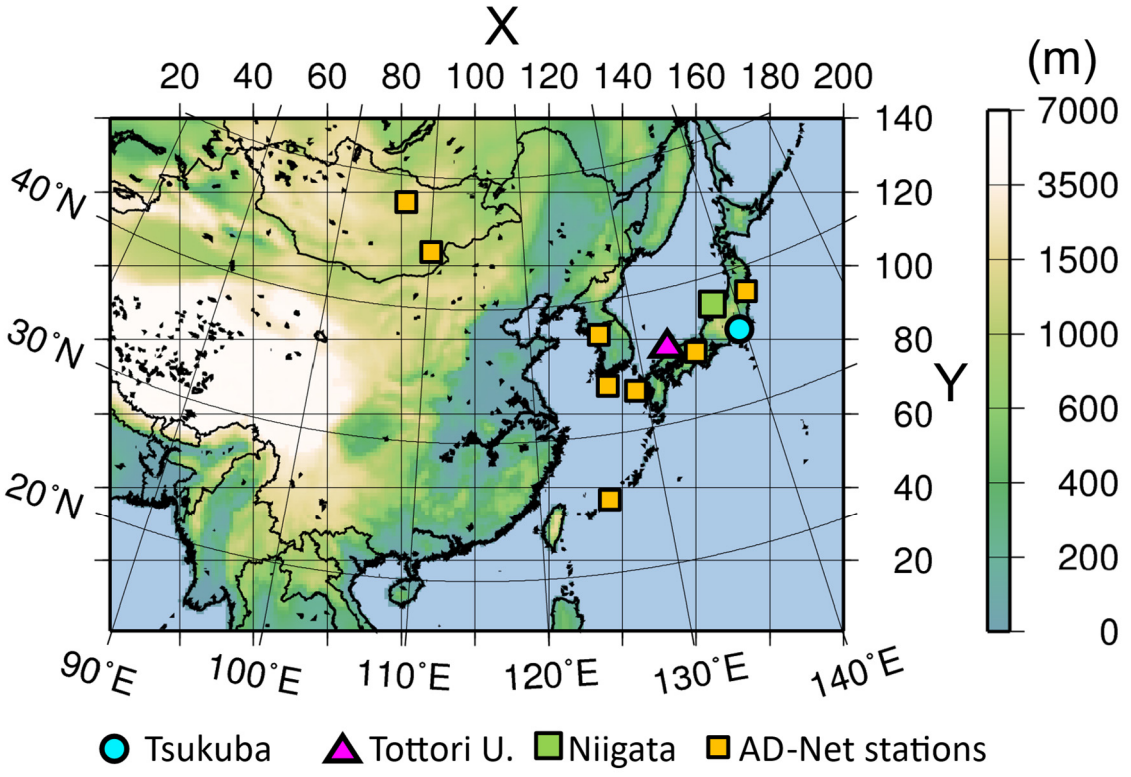

Figure 2: Model domain, terrestrial elevation, and observation sites used in this study.

2.2 Observation data

2.2.1 Scanning mobility particle sizer and aerodynamic particle sizer

Aerosol size distributions were measured with a SMPS (Model 3936L75, TSI Inc.) and an APS (Model 3321, TSI Inc.) on the MRI campus in Tsukuba (140.125°E, 36.056°N, X = 173, Y = 86, 24 m m.s.l.) (Orikasa et al., 2020). Ambient air was sampled through a PM_{10} inlet located 11 m above ground level (a.g.l.) at a flow rate of 120 L min^{-1} via a stainless-steel line (internal diameter 7 cm). The sampled air was dried with a diffusion dryer packed with silica gel before entering the SMPS and APS. The SMPS measured submicron number size distributions with 105 bins covering 10–400 nm mobility diameter; the full range was scanned every 120 s. Sheath and sample flows were 6.3 and 0.63 L min^{-1}, respectively. The APS measured supermicron number size distributions with 52 bins spanning 0.5–20 µm aerodynamic diameter; the full range was scanned every 60 s, with sheath and sample flows of 4 and 1 L min^{-1}, respectively.

Hourly time series of number size distributions for July–December 2015 and January–June 2016 are shown in Figs. A1 and A2; monthly mean size distributions for July 2015–June 2016 appear in Fig. A3. Hourly and daily averaged data were used for model evaluation.

https://doi.org/10.5194/egusphere-2026-1666
Preprint. Discussion started: 27 May 2026

APS data require careful handling (e.g., Martin et al., 2010; Pfeifer et al., 2016; Gregson et al., 2021). Martin et al. (2010) reported consistency between APS and an optical particle counter (OPC) in the 0.8–5 μm range. Pfeifer et al. (2016) compared 15 APS Model 3321 units and found unit-to-unit variability of 10%–20% for particles of 0.9–3 μm, increasing to ~60% below 0.9 μm due to counting-efficiency differences; variability can exceed 100% above 3 μm (Pfeifer et al., 2016). In this study, after comparing APS and SMPS data, APS data below 1 μm were excluded from model evaluation (see Sect. 2.3.4). APS data for larger particles (> 3–5 μm) were retained because alternative validation data (for example, OPC) were unavailable.

The APS artifact at smaller aerodynamic sizes (below 1 μm) is evident in Fig. A3 and later in Fig. 4. In APS panels M_2 and M_3 (Figs. A3f and A3i), SMPS-derived data, converted assuming $\rho_p = 1.8\times10^3$ kg m^{-3}, are plotted as open circles. Even accounting for density uncertainty, SMPS values remain substantially higher than APS in the 0.4–0.5 μm range, whereas SMPS and APS curves tend to converge near ~0.7 μm. This motivated the exclusion of APS data below 1 μm from our analysis.

2.2.2 Other data (lidar and ion chromatography)

To evaluate NHM-Chem v2.0 improvements inferred from SMPS and APS, we used two independent observational datasets: the Asian dust and aerosol lidar observation network (AD-Net) and ion chromatography data measured at Tottori University.

AD-Net is a lidar network for continuous vertical observations of Asian dust and other aerosols across East Asia, operated by the National Institute for Environmental Studies (NIES) in Tsukuba. AD-Net data are archived at NIES (http://www-lidar.nies.go.jp/AD-Net/; last access: 2 March 2026). NIES and MRI are adjacent laboratories. As depicted in squares in Fig. 2, among AD-Net stations, we used data from Chiba (140.10°E, 35.63°N, nearest model X = 173, nearest model Y = 84), Fukue (128.68°E, 32.75°N, X = 142, Y = 66), Fukuoka (130.48°E, 33.52°N, X = 147, Y = 70), Hedo (128.25°E, 26.87°N, X = 145, Y = 44), Jeju (126.16°E, 33.29°N, X = 135, Y = 67), Matsue (133.01°E, 35.21°N, X = 154, Y = 77), Nagasaki (129.98°E, 32.84°N, X = 146, Y = 67), Niigata (138.94°E, 37.84°N, X = 168, Y = 91), Osaka (135.59°E, 34.65°N, X = 162, Y = 77), Sainshand (110.12°E, 44.87°N, X = 88, Y = 106), Sendai (140.85°E, 38.25°N, X = 172, Y = 94), Seoul (126.95°E, 37.46°N, X = 135, Y = 82), Toyama (137.1°E, 36.7°N, X = 164, Y = 85), Tsukuba (NIES campus, 140.12°E, 36.05°N, X = 173, Y = 86), and Ulaanbaatar (106.90°E, 47.92°N, X = 81, Y = 118). (Note: closely spaced stations are represented by single map symbols in Fig. 2; for example, Chiba and Tsukuba, Toyama and Niigata, Fukue, Nagasaki, and Fukuoka). The standard AD-Net lidar is a two-wavelength (1064 and 532 nm) system with polarization sensitivity at 532 nm (Sugimoto et al., 2008; Shimizu et al., 2016). Attenuated backscattering coefficients at 1064 and 532 nm and the volume depolarization ratio at 532 nm are available at 15-min intervals and vertically up to 18,000 m a.g.l. with 6-m height resolution. Extinction coefficients for nonspherical (dust) and spherical aerosols are derived from the backscattering and depolarization ratios (Sugimoto et al., 2003; Shimizu et al., 2004) at 30-m intervals up to 9,000 m a.g.l. In this study, we used dust aerosol optical depth (AOD) and spherical AOD for model validation. Because of insufficient overlap between the

https://doi.org/10.5194/egusphere-2026-1666
Preprint. Discussion started: 27 May 2026

laser beam and the telescope field of view, the extinction coefficient in the lowest four layers (ground to 120 m) is treated as missing data. Consequently, simulated AOD was computed by accumulating simulated extinction coefficients while excluding the lowest two model layers (the top of the model's second layer is ~126 m a.g.l.). Because the lidar cannot retrieve AOD in cloudy grid boxes, model column AODs for grids where total hydrometeor mixing ratios (cloud, rain, ice, snow, and graupel) exceeded 1×10^{-6} kg kg^{-1} were excluded. Hourly and daily averages were used for evaluation.

Ion concentrations of fine-mode ($PM_{2.5}$) and coarse-mode ($PM_{2.5}$–PM_{10}) particles measured at Tottori University (134.22°E, 35.53°N, X = 157, Y = 79) (Nojiri et al., 2022) were used (see triangle in Fig. 2). Hourly mass concentrations of the fine and coarse-mode particles collected on polytetrafluoroethylene (PTFE) tape filters were measured by beta attenuation (PM-712; Kimoto Electric Co., Ltd.). The PTFE tape filter of the PM-712 was covered with polyester tape during storage to avoid contamination. Ionic compositions of particulate matter (PM) spots on the PTFE filters were analyzed by ion chromatography. Time resolution of the ionic-composition data ranged from 4 to 24 h, depending on PM mass loading. Simulation data were averaged to match the observation time resolution for comparison.

Because the Tottori University site is coastal, some aerosol components include sea-salt contributions. To estimate non-sea-salt (nss) SO_4^{2-} and Ca^{2+} (the latter as a tracer for Asian dust composed of calcite), we subtracted sea-salt contributions using standard seawater composition:

$$[\text{nss-}SO_4^{2-}] = [SO_4^{2-}] - 0.251 \times [Na^+],$$

$$[\text{nss-}Ca^{2+}] = [Ca^{2+}] - 0.038 \times [Na^+],$$

where [ ] denotes weight concentrations in μg m^{-3}.

https://doi.org/10.5194/egusphere-2026-1666
Preprint. Discussion started: 27 May 2026

Table 1: List of PPVs for the evaluation of simulated aerosol processes and properties using size-resolved measurement data.

Symbols	Description [unit]	Measurement data and assumptions		
PPVs derived and used for model evaluation in this study.				
		SMPS_SUB	APS_MD	APS_SS
Condensation				
$\varphi(\kappa)$	Mass transport coefficient of H_2SO_4 gas to ambient sizes of aerosol particles of hygroscopicity κ [s^{-1}]	$\kappa = 0.3$	$\kappa = 3.385 \times 10^{-4}$	$\kappa = 1.2$
Coagulation				
$\beta(\kappa, D)$	Coagulation rate of monodisperse aerosol particles of dry diameter D and number concentrations 10^6 m^{-3} to ambient sizes of aerosol particles [m^3 s^{-1}]	$D = 1$ nm $D = 9$ nm	$D = 1$ nm $D = 9$ nm	$D = 1$ nm $D = 9$ nm
Cloud condensation nuclei				
$N_{CCN}(\kappa, S_s)$	CCN number concentrations at supersaturation S_s [m^{-3}]	$S_s = 0.1\%$ $S_s = 1.0\%$	$S_s = 0.1\%$ $S_s = 1.0\%$	$S_s = 0.1\%$ $S_s = 1.0\%$
Optical properties				
$\sigma_{ext}(\kappa, \lambda, m)$	Light extinction coefficient of ambient sizes of aerosol particles at wavelength λ and refractive indices of aerosol component m_a and aerosol water m_w [m^{-1}]	$\lambda = 532$ nm $m_a = 1.53 + 1.00\times10^{-9}i$ $m_w = 1.33 + 1.61 \times 10^{-9}i$	$\lambda = 532$ nm $m_a = 1.53 + 6.33\times10^{-3}i$ $m_w = 1.33 + 1.61 \times 10^{-9}i$	$\lambda = 532$ nm $m_a = 1.50 + 1.00 \times 10^{-9}i$ $m_w = 1.33 + 1.61 \times 10^{-9}i$
PPVs proposed but not used in this study.				
Optical properties				
$\sigma_{abs}(\kappa, \lambda, m)$	Light absorption coefficient			
$\sigma_{sca}(\kappa, \lambda, m)$	Light scattering coefficient			
Ice nucleation				
$N_{INP}(n_s, T_f)$	Number concentrations of ice nucleating particles (INPs) with ice nucleation active site (INAS) density n_s as a function of freezing temperature T_f.			
In-cloud scavenging				
$V_{CCN}(\kappa, S_s)$	Activated volume concentrations at supersaturation S_s [m^3 m^{-3}]			
Below-cloud scavenging				
$\Lambda(\kappa,P)$	Below the cloud scavenging rate by (liquid or solid) precipitation at a rate of P [s^{-1}]			
Dry deposition velocity				
$V_d(\kappa,U)$	Dry deposition velocity of aerosols at surface wind U m s^{-1} over (smooth or rough surfaces [m s^{-1}]			

https://doi.org/10.5194/egusphere-2026-1666
Preprint. Discussion started: 27 May 2026

2.3 Derivation of pseudo-physical variables (PPVs)

2.3.1 Pseudo-physical variables (PPVs)

Table 1 lists the PPVs proposed in this study.

To evaluate condensational growth and evaporation processes of aerosol particles, we derived a gas-to-particle mass-transport coefficient, φ (s^{-1}). φ is important for new particle formation because a larger φ implies a larger condensational sink for sulfuric acid (or extremely low-volatility organics, ELVOCs), which reduces the nucleation rate as a function of the number concentration of sulfuric acid gas (or ELVOC) molecules. We calculate φ as

$$\varphi = \int_{D_{\min}}^{D_{\max}} 2\pi D_{\mathrm{v}} D_{\mathrm{w}} n(\log D) f(\mathrm{Kn}, \alpha) d\log D \quad , \tag{1}$$

where D is the dry diameter, D_{min} and D_{max} are the minimum and maximum diameters, $n(\log D)$ is the number size distribution, and $d\log D$ is the logarithmic size increment (from SMPS or APS). D_v is the molecular diffusivity of sulfuric acid gas. The mean wet (or ambient) diameter, D_w, is calculated by iteratively solving the relation among growth factor G (D_w/D), hygroscopicity κ, and relative humidity (RH) from the κ-Köhler formulation (Petters and Kreidenweis, 2007):

$$\frac{RH}{exp\left(\frac{A}{DG}\right)} = \frac{G^3 - 1}{G^3 - (1 - \kappa)} \quad . \tag{2}$$

where A accounts for the Kelvin (curvature) effect:

$$A = \frac{4\sigma_{\mathrm{s/a}} M_{\mathrm{w}}}{RT\rho_{\mathrm{w}}} \quad , \tag{3}$$

with $\sigma_{\mathrm{s/a}}$ the solution–air surface tension (set as 0.072 J m^{-2}), M_{w} the molecular weight of water, R the universal gas constant, T temperature, and ρ_{w} water density. The transition-regime correction factor $f(\mathrm{Kn}, \alpha)$ (Fuchs and Sutugin, 1971) is

$$f(Kn, \alpha) = \frac{0.75\alpha(1 + \mathrm{Kn})}{\mathrm{Kn}(1 + \mathrm{Kn}) + 0.283\alpha\mathrm{Kn} + 0.75\alpha} \quad , \tag{4}$$

where Kn is the Knudsen number (defined as $\mathrm{Kn} = 2\lambda_{\mathrm{g}}/D_{\mathrm{w}}$, and λ_{g} is the mean free path of sulfuric acid gas), and α is the accommodation coefficient (0.1 in this study).

To evaluate coagulation growth, we compute a coagulation rate β (m^3 s^{-1}) for aerosol particles of a specified size (D_{fix}) and number concentration n_{fix} as

$$\beta = \int_{D_{\min}}^{D_{\max}} K(D_{\mathrm{fix}}, D_{\mathrm{w}}) n_{\mathrm{fix}} n(\log D) d\log D \quad , \tag{5}$$

where $K(D_{\mathrm{i}}, D_{\mathrm{j}})$ is the Brownian coagulation kernel between two sizes of aerosols D_{i} and D_{j} for the transition regime (Fuchs, 1964; Jacobson, 2005), defined as:

https://doi.org/10.5194/egusphere-2026-1666
Preprint. Discussion started: 27 May 2026

$$K(D_i, D_j) = \frac{2\pi(D_i + D_j)(D_{pi} + D_{pj})}{\frac{(D_i + D_j)}{2}} \quad , \quad (6)$$

where D_p is the Brownian diffusion coefficient of a particle, δ is the mean distance from the center of a sphere reached by a particle leaving the sphere's surface and traveling a distance of the particle's mean free path, and $\bar{v}_p$ is the thermal speed of a particle in the air. In this study, we set n_{fix} = 1×10^6 m^{-3}, and evaluate β at D_{fix} = 1 nm and 9 nm, corresponding to new-particle sizes in NHM-Chem v1.0 and v2.0, respectively. β is a key parameter for new particle formation (NPF) because large β implies efficient coagulation sink and reduced survival of newly nucleated particles.

To evaluate the cloud condensation nuclei (CCN) activation, we calculate the activated number concentration of aerosols at supersaturation S_s,

$$N_{CCN}(S_s) = \int_{D_c(S_s,\kappa)}^{D_{max}} n(\log D) d\log D \quad , \quad (7)$$

where the critical dry diameter $D_c(S_s, \kappa)$ is obtained from κ-Köhler theory (Petters and Kreidenweis, 2007). The saturation ratio as a function of wet diameter is

$$s(D_w) = \frac{D_w^3 - D^3}{D_w^3 - D^3(1-\kappa)} exp\left(\frac{A}{D_w}\right) \quad , \quad (8)$$

where $s(D_w)$ is the saturation ratio, and the critical saturation ratio s_c is the maximum of Eq. (8) for $D_w > D$. For a given S_s (where $S_s = s_c - 1$), D_c is the smallest dry diameter satisfying $s_c - 1 > S_s$. We evaluate S_s = 0.1% and S_s =1.0% as representative of stratiform and convective cloud-base conditions.

To evaluate aerosol–radiation interactions, the light extinction coefficient is calculated as

$$\sigma_{ext}(\lambda) = \int_{D_{min}}^{D_{max}} \frac{\pi}{4} q_{ext}(D_w, \lambda, m) D_w^2 n(\log D) d\log D \quad , \quad (9)$$

where $\sigma_{ext}(\lambda)$ is the extinction coefficient (m^{-1}) at a wavelength λ, q_{ext} is the efficiency factor for light extinction calculated by the Mie theory as a function of D_w, λ, and refractive index m. We use λ = 532 nm to match AD-Net lidar observations.

The above PPVs are derived and evaluated in this study, but other PPVs can be proposed, as listed in Table 1. To validate in-cloud scavenging processes, the activated volume of aerosols activated as CCN at S_s,

$$V_{CCN}(S_s) = \int_{D_c(S_s,\kappa)}^{D_{max}} \frac{\pi}{6} D^3 n(\log D) d\log D \quad , \quad (10)$$

can be proposed. Similarly, the number concentration of ice nucleating particles N_{INP}, below the cloud scavenging rate Λ, or dry deposition velocity v_d can be derived and compared. The scattering coefficient $\sigma_{sca}(\lambda)$ and absorption coefficient $\sigma_{abs}(\lambda)$

https://doi.org/10.5194/egusphere-2026-1666
Preprint. Discussion started: 27 May 2026

can also be good indicators of consistent predictions of aerosol-radiation interaction processes, such as direct and semi-direct effect of aerosols.

2.3.2 Moments

Here, *the k*-th moment of aerosols is defined as

$$M_k = \int_{D_{\min}}^{D_{\max}} D^k n(\log D) d\log D \quad . \tag{11}$$

When D^k (or D_w^k) is applied in Eq. (11), *the k*-th moment of dry aerosols $M_{k,\mathrm{dry}}$ (or wet aerosols $M_{k,\mathrm{wet}}$) is obtained. Zeroth, second, and third moments (M_0, M_2, *and* M_3) are the same as total number concentration (N_{tot}), proportional to surface area concentration ($=\pi M_2$), and proportional to volume concentration ($=\pi/6 M_3$), respectively. PPVs can be derived and compared as absolute values, whereas PPVs relative to any moments ($M_{k,\mathrm{dry}}$ or $M_{k,\mathrm{wet}}$) can be used to apply. For example, deviations in absolute values, such as N_{CCN} and σ_{ext}, directly affect the accuracy in the aerosol-cloud interaction and aerosol-radiation interaction processes in aerosol-to-meteorology feedback simulations. On the other hand, even though N_{CCN} and σ_{ext} are consistent, the overall simulation is not consistent if there are huge deviations in mass concentrations. To obtain a consistent size distribution of aerosols in the simulation, the PPVs to mass (or volume) ratio must be consistent. In this study, both PPVs relative to volume (or third moments) and the absolute PPVs are derived and compared in the main body and supplement, respectively (see Sect. 5).

2.3.3 SMPS_SUB

Simulated and observed φ, β, N_{CCN}, and $\sigma_{\mathrm{ext}}(\lambda)$ were calculated from SMPS data assuming typical properties of hygroscopic submicron particles (SMPS_SUB). The simulated lognormal dry number size distributions for the five aerosol categories were discretized into the 105 SMPS bins ($D_{\min}$ = 9.47 nm to $D_{\max}$ = 399.5 nm mobility diameter), assuming spherical particles (shape factor = 1) and that mobility diameter equals geometric diameter (D) (Rupakheti et al., 2005). We set κ = 0.3 (size-independent), representing an inorganic–organic mixture. For κ = 0.3 at T = 293.15 K, D_c = 168 nm for S_s = 0.1% and D_c = 36.2 nm for S_s = 1.0%. Refractive indices follow the Optical Properties of Aerosols and Clouds (OPAC) library (Hess et al., 1998). The refractive index m of submicron dry aerosols is set as a water-soluble (WASO) component of OPAC, $1.53+1.00\times10^{-9}i$, and that of aerosol water as fog (FOGR), $1.33+1.61\times10^{-9}i$ at λ = 532 nm. The refractive index of wet aerosols was computed by volume weighting: $v_{\mathrm{dry}} m_{\mathrm{WASO}} + (1 - v_{\mathrm{dry}}) m_{\mathrm{FOGR}}$, where v_{dry} is the volume fraction of dry aerosols. Standard pressure (101,325 Pa) was assumed; however, simulated and observed T and RH were used in PPV calculations for simulated and observed cases, respectively, so that meteorological bias could affect PPVs comparisions.

https://doi.org/10.5194/egusphere-2026-1666
Preprint. Discussion started: 27 May 2026

Typical T deviations were ~1 K, representing a negligible ratio to absolute temperature (~1 K/300 K) and a <1% effect on PPVs. Conversely, RH deviations can reach ~10% and substantially affect PPVs at high RH (except for N_{CCN} determined by dry diameter), because dG/dRH increases rapidly at high RH (for κ = 0.3, $G \approx$ 1.2, 1.3, 1.5, 2.0, 3.2, and 7.5 at RH levels of 70%, 80%, 90%, 96%, 99%, and 99.9%, respectively). To avoid large deviations in G at high RH, both simulated and observed RH values were set to a maximum of 96% to calculate PPVs.

2.3.4 APS_MD and APS_SS

Coarse-mode particles are dominated by dust and sea salt, which differ physically: dust tends to be hydrophobic and light-absorbing, whereas sea salt is hygroscopic and non-light-absorbing. For APS data, we therefore computed two PPV variants assuming 100% mineral dust (APS_MD) and 100% sea salt (APS_SS).

The APS provides 52 bins from 0.392 μm to 19.81 μm aerodynamic diameter, but we used only APS data >1 μm. Reasons: (1) Submicron PPVs are validated using SMPS. (2) APS counting efficiency at small aerodynamic diameters can be unreliable (see Sect. 2.2.1), as the APS artifact is apparent in Figs. 4f, 4h, A3f, and A3i: APS values in the 0.4–0.5 μm range are substantially smaller than SMPS values, assuming that the relationship between the aerodynamic diameter D_a and mobility diameter D_m is $D_a = D_m\sqrt{\rho_p}$, where particle density $\rho_p = 1.8\times10^3$ kg m^{-3}.

For APS_MD, simulated lognormal dry number distributions for the five categories were discretized into 42 APS bins covering D_{min} = 1.037 μm to D_{max} = 19.81 μm aerodynamic diameter. We assumed spherical particles and $\rho_p = 2.6\times10^3$ kg m^{-3} to convert aerodynamic diameter D_a to geometric diameter D via $D = D_a/\sqrt{\rho_p}$. We set κ for mineral dust to 3.385×10^{-4}, which approximates wetting behavior near that of hydrophobic particles ($\kappa \approx 0$) when exposed to pure water (see Fig. 1 of Petters and Kreidenweis, 2007). For $\kappa = 3.385\times10^{-4}$ at T = 293.15 K, D_c = 1.61 μm for S_s = 0.1% and D_c = 348 nm for S_s = 1.0%. The refractive index m of mineral dust was set to $1.53+6.33\times10^{-3}i$ (mineral dust of OPAC, MIAM) at λ = 532 nm, and the m of wet aerosols was computed by volume weighting as in SMPS_SUB. For APS_SS, PPVs were computed similarly but with κ = 1.12, $\rho_p = 2.2\times10^3$ kg m^{-3}, and m of sea salt = $1.50+10^{-9}i$ (sea salt of OPAC, SSAM). For κ = 1.12 at T = 293.15 K, D_c = 108 nm for S_s = 0.1% and D_c = 23.3 nm for S_s = 1.0%.

3 Development of NHM-Chem v2.0 based on the evaluation of the Extinction-to-Volume Ratio (EVR).

Among the PPVs, the extinction-to-volume ratio (EVR) ($\sigma_{ext}(\lambda)/(\pi/6M_3)$) is particularly important because many aerosol analysis products assume that the extinction-to-mass relationship of forward models is exact (Innes et al., 2013; Buchard et al., 2015; Flemming et al., 2017; Yumimoto et al., 2017). Satellite-derived AOD is widely used for data assimilation to adjust aerosol mass concentrations; EVR therefore plays a central role in improving predictions of aerosols' direct and semi-

https://doi.org/10.5194/egusphere-2026-1666
Preprint. Discussion started: 27 May 2026

direct climate effects. For the v1.0 to v2.0 update of NHM-Chem, EVR was selected as the top PPV priority for improvement.

3.1 Differences in modules and settings of NHM-Chem v1.0 and v2.0 for aerosol size distributions

The major v2.0 update relative to v1.0 is that online meteorology–chemistry coupling and aerosol–meteorology feedback are implemented (Kajino et al., 2026). Improving aerosol size-distribution simulations is the principal focus of this study. Other important differences between the two versions of NHM-Chem (aside from minor bug fixes) are: (1) changes in emitted aerosol size parameters, (2) inclusion of additional heterogeneous reactions, and (3) implementation of the parameterization of Kerminen and Kulmala (2002). The Kerminen–Kulmala implementation is described in Sect. 3.3; items (1) and (2) are summarized here.

In the model, size parameters such as D_g and σ_g must be prescribed in boundary and emission conditions. As described in Kajino et al. (2019), for example, aerosols are categorized into ATK, ACM, AGR, SS, and DU in the five-category dynamic method, ATK, ACM (accumulation mode both soot-free and mixed-with-soot), and COR (coarse mode including sea-salt and dust) in the three-category dynamic method, and SUB (submicron modes), DU, and SS in the bulk equilibrium method. In v1.0, (D_g, σ_g) pairs prescribed for the ATK and accumulation (ACM, AGR, and SUB) modes (both emissions and lateral/upper boundaries) were (10 nm, 1.3) and (100 nm, 1.5) in number-equivalent dry aerodynamic diameter, respectively. After sensitivity tests varying boundary-condition size parameters, we found better agreement of simulated EVR (Fig. 3) and size distributions (Fig. 4) with observations when v2.0 was used (D_g, σ_g) = (10 nm, 1.3) for ATK and (100 nm, 1.8) for accumulation modes, expressed as number-equivalent dry real diameter. Coarse mode (DU, SS, and COR) size parameters were also adjusted by the same sensitivity tests to improve simulated EVR. In v1.0, (D_g, σ_g) for DU, SS, and COR were (2.0 µm, 1.8), (1.0 µm, 1.8), and (1.0 µm, 1.8), respectively, in number-equivalent dry aerodynamic diameter. In v2.0, (D_g, σ_g) of DU was changed to (1.0 µm, 1.8). Note that for mineral dust and sea salt, size parameters are calculated or assumed by the emission schemes, so that the prescribed values above apply to anthropogenic dust emissions and to lateral/upper boundary conditions for total dust (mineral + anthropogenic) and sea salt. In v1.0, mineral dust emission size parameters varied with vegetation or surface soil category (Han et al., 2004; Ishizuka et al., 2017). In v2.0, we simplified these to constant emission parameters: D_g = 1.0 µm and σ_g = 1.8 (number-equivalent dry aerodynamic diameter) for mineral dust. Similarly, sea-salt emission size parameters were set constant at (D_g, σ_g) = (1.0 µm, 1.8) in v2.0. These emission and boundary size parameters are provisional and will be refined as additional observations become available.

In v1.0, three heterogeneous reactions from Jacob (2000) were included. Because models tend to overestimate total nitrate (gas + aerosol) or $PM_{2.5}$-nitrate in East Asia (Kajino et al., 2013b; Shimadera et al., 2013; Kajino et al., 2019), we included two additional reactions in v2.0, following Li et al. (2015) and Andersen et al. (2023):

https://doi.org/10.5194/egusphere-2026-1666
Preprint. Discussion started: 27 May 2026

$$HNO_3 + (soot) \rightarrow 0.5\ NO + 0.5\ NO_2 \quad , \quad (R1)$$

$$NO_3^-(p) + h\nu \rightarrow 0.67\ HONO + 0.33\ NO_2 \quad , \quad (R2)$$

However, inclusion of these two reactions did not substantially improve nitrate or related species (for example, O_3); further additional heterogeneous processes are being tested. The sensitivity studies and related model improvements will be summarized in a future paper; for the present study, we used the five heterogeneous reactions described above.

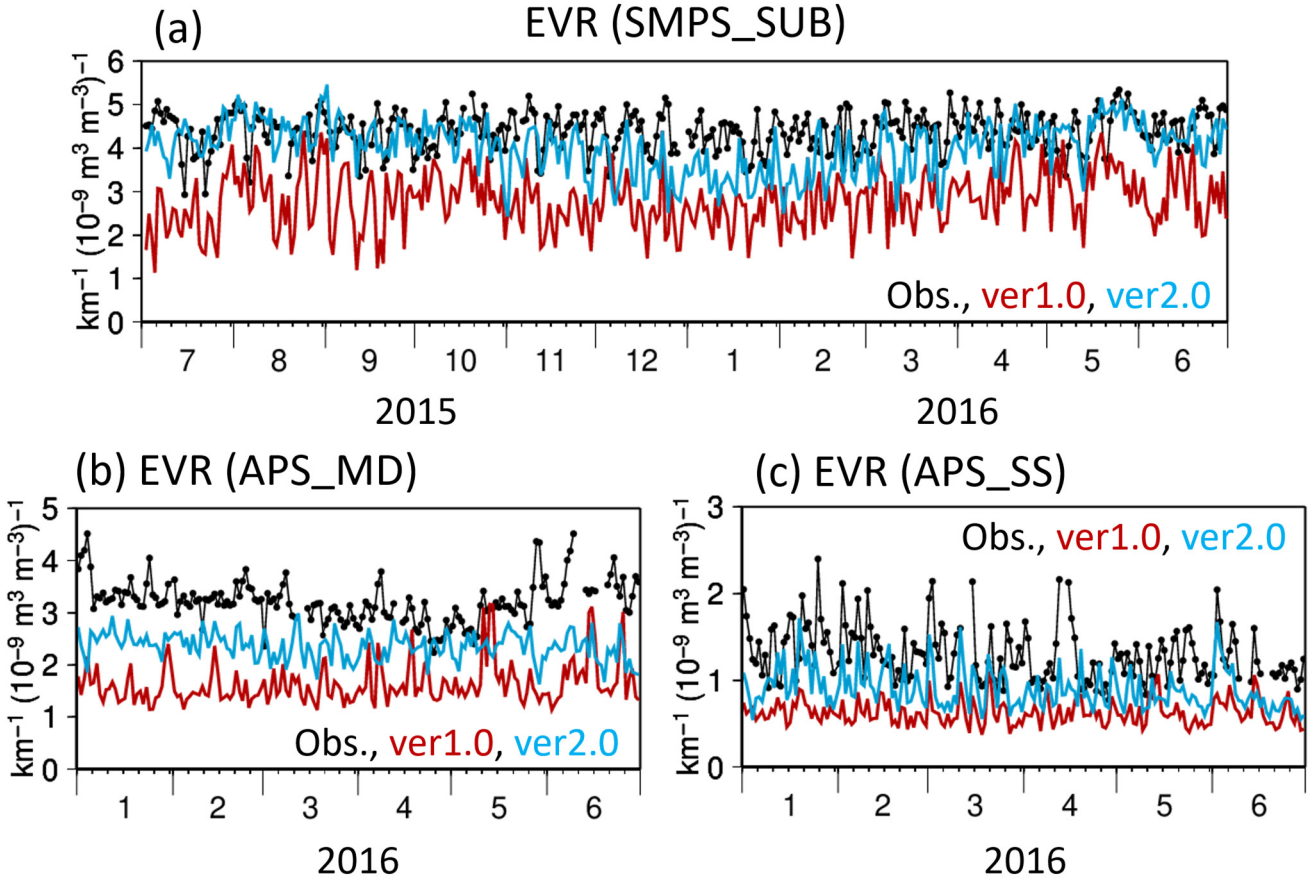

Figure 3: Time series of (black) observed and (colors) simulated (red: NHM-Chem v1.0, cyan: NHM-Chem v2.0) daily extinction to volume ratio (EVR) by assuming (a) submicron particles from July 2015 to June 2016 over all SMPS size bins (SMPS_SUB), and (b) mineral dust particles over APS size bins above 1 μm (APS_MD), and (c) sea salt particles over APS size bins above 1 μm (APS_SS) from January to June 2016.

https://doi.org/10.5194/egusphere-2026-1666
Preprint. Discussion started: 27 May 2026

Table 2: Statistical scores comparing hourly simulated and observed EVR (km^{-1} (10^{-9} m^3 m^{-3}) $^{-1}$) shown in Fig. 3.

PPVs	Measurement data and assumptions	*R*[a] (v2.0/v1.0)	*Sim./Obs.*[b] (v2.0/v1.0)	*Observed median*	*RMSE*[c] (v2.0/v1.0)
EVR	SMPS_SUB	0.21/0.16	0.95/0.65	4.29	0.90/1.77
	APS_MD	0.0020/0.15	0.76/0.48	3.18	1.02/1.70
	APS_SS	0.60/0.44	0.64/0.46	1.56	0.64/0.95

[a]Correlation coefficients
[b]Simulated median to observed median ratio
[c]Root mean square error

3.2 Comparison of the EVR and aerosol size distribution

Figure 3 shows the daily observed and simulated EVR at λ = 532 nm for SMPS_SUB, APS_MD, and APS_SS. Hourly statistical scores are summarized in Table 2. Overall, v2.0 substantially improved *Sim./Obs.* and *RMSE* for all three PPV categories compared with v1.0. Because coarse-mode size distributions change slowly in the atmosphere, improvements in simulated EVR for APS_MD and APS_SS are likely attributed to changes in emitted size parameters and boundary conditions (Sect. 3.1). Conversely, submicron size distributions evolve rapidly (from a few nanometers to several hundred nanometers) in the atmosphere; therefore, improving SMPS_SUB EVR required not only changes in emission and boundary size parameters but also improvements in the parameterizations governing size-evolution processes (Sect. 3.3; Fig. 5).

For SMPS_SUB, v1.0 underestimated EVR by 35%; v2.0 increased *Sim./Obs.* to 0.95 (near unity). For coarse modes v2.0 *Sim./Obs.* remained below unity (0.76 for APS_MD and 0.64 for APS_SS), though both improved from v1.0 (0.48 and 0.46 for APS_MD and APS_SS, respectively). Because of known APS limitations at smaller sizes (Sect. 2.2.1), we did not attempt further tuning to force *Sim./Obs.* ratios for APS_MD and APS_SS upward. Temporal correlation *R* between simulated and observed EVR was generally poor except for APS_SS. The better correlation for APS_SS likely reflects two factors used in both model and observation-derived EVR: (i) sea-salt particles have a high hygroscopicity ($\kappa \approx 1.2$) that yields strong, consistent *RH*-driven growth, and (ii) there were fairly good correlation between simulated and observed *RH*.

https://doi.org/10.5194/egusphere-2026-1666
Preprint. Discussion started: 27 May 2026

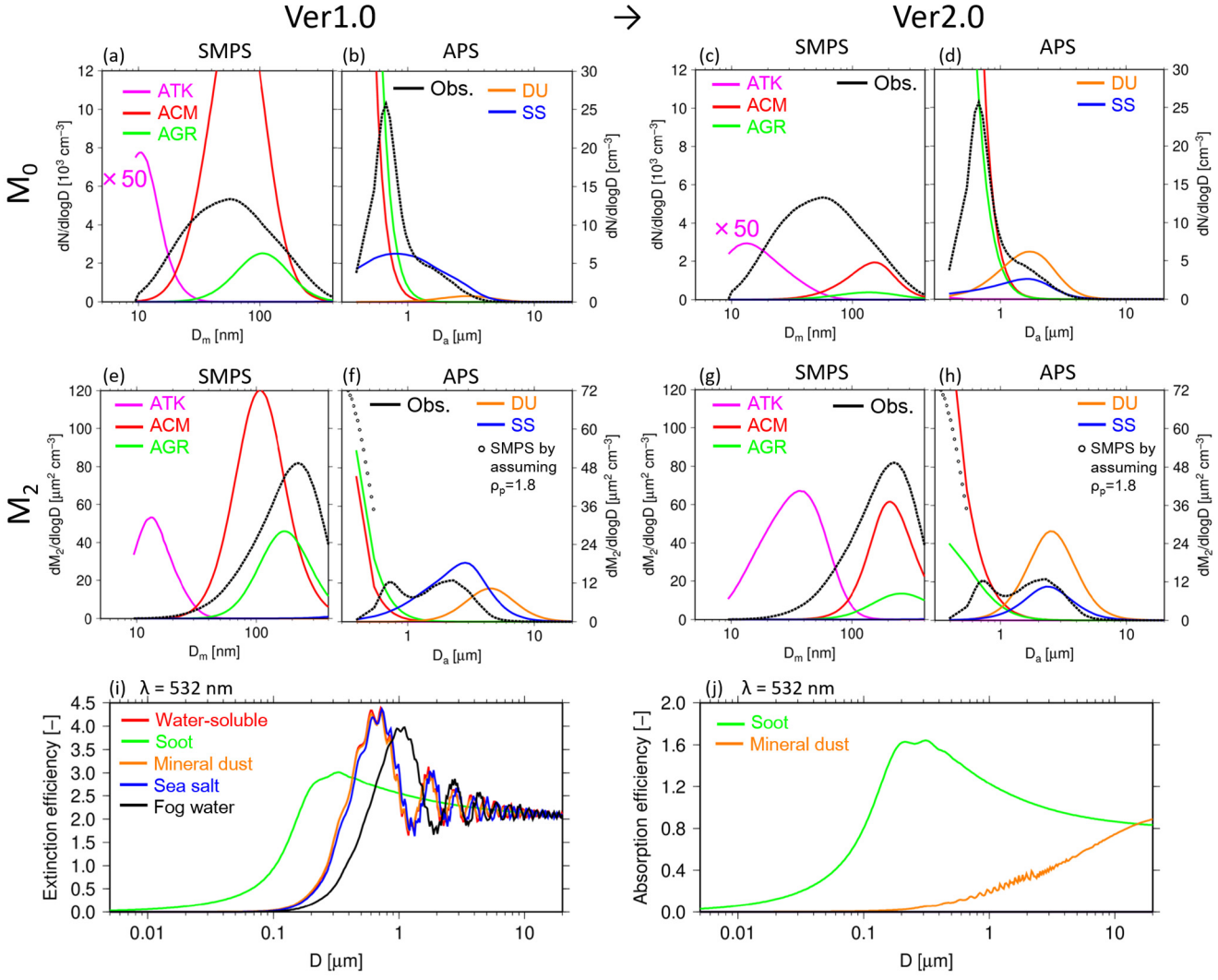

Figure 4: (a–h) (black) observed and (colors) simulated seasonal mean (a–d) number (zeroth moment; M_0) and (e–h) second moment (M_2) size distributions of aerosols in March, April, and May 2016. The color lines represent size (dry) distributions of five categories of NHM-Chem, namely, (pink) Aitken mode (ATK), (red) soot-free accumulation mode (ACM), (lime) internally mixed with soot aggregate (AGR), (orange) dust (DU), and (blue) sea salt (SS), discretized in (a, c, e, g) SMPS bins and (b, d, f, h) APS bins, simulated by (a, b, e, f) v1.0 and (c, d, g, h) v2.0. Note that the number size distributions of ATK (a, c) are 50 times greater than the y-axis. In the APS panels, SMPS data are also depicted as open circles by assuming the following conversion, $D_a = D_m\sqrt{\rho_p}$, where particle density $\rho_p = 1.8\times10^3$ kg m^{-3}. (i) Extinction efficiencies of (red) water-soluble, (lime) soot, (orange) mineral dust, (blue) sea salt, and (black) fog water aerosols, with refractive indices of $1.53 + 1.00 \times 10^{-9}i$, $1.95 + 0.79i$, $1.53 + 6.33 \times 10^{-3}i$, $1.50 + 1.00 \times 10^{-9}i$, and $1.33 + 1.61 \times 10^{-9}i$, respectively, at a wavelength of 532 nm (Hess et al., 1998). (j) Absorption efficiencies of (lime) soot and (orange) mineral dust at a wavelength of 532 nm.

https://doi.org/10.5194/egusphere-2026-1666
Preprint. Discussion started: 27 May 2026

Figure 4 shows the seasonal mean (spring: March–May 2016) simulated and observed M_0 and M_2 size distributions over SMPS and APS bins. The extinction and absorption efficiencies of typical aerosol components are shown in Figs. 4i and 4j, respectively. Fig. 4 visually explains the simulated and observed features presented in Fig. 3.

The simulated number size distributions of coarse-mode particles (DU and SS) generally agree with observations (Fig. 4b), but the simulated M_2 peak diameters of DU and SS were overestimated in v1.0 (Fig. 4f), causing simulated EVR to be underestimated (for the same volume, larger particles produce less light extinction). After model improvements, the simulated M_2 peak diameters of DU and SS became consistent with observations. Although DU and SS size distributions should differ, they cannot be separately validated with the current SMPS–APS setup; instead, we evaluate their consistency using independent datasets, such as dust AOD from the AD-Net lidar and $PM_{2.5}/PM_{10}$ ratios of nss-Ca^{2+} and Na^{+} (see Sect. 4).

For submicron particles (ATK, ACM, and AGR), adjusting emitted size parameters is not straightforward because atmospheric processes rapidly grow sizes from a few nanometers to several hundred nanometers. NPF injects large numbers of nanoparticles into ATK, which then grow into ACM by condensation and coagulation. Condensational growth of AGR particles depends on the relative surface-area concentrations of ATK, ACM, and AGR, since condensation rate is proportional to M_2 in the free-molecular regime (e.g., Kajino et al., 2013a). In v1.0, the simulated M_0 peak diameters for ACM and AGR were within reasonable ranges of the observations (Fig. 4a), but the simulated M_2 peak diameter of ACM (~100 nm) was substantially smaller than observed (~250 nm) (Fig. 4e); the simulated M_2 peak diameter of AGR (~180 nm) was slightly smaller than observed. These differences in peak diameters were critical for accurate light-extinction predictions. Figs. 4i and 4j show that, except for soot (in AGR), particles smaller than ~100 nm minimally interact with 532 nm light. Extinction efficiencies for non-soot components rise steeply with size: ~0.0 at D = 100 nm, ~0.5 at D = 200 nm, ~1.5 at D = 300 nm, ~2.5 at D = 400 nm, and ~4.0 at D = 500 nm. Therefore, aerosol size distributions in the 100–500 nm range are critically important for accurate EVR predictions. The substantially smaller ACM M_2 peak diameter in v1.0 explains the SMPS_SUB EVR underestimation in Fig. 3a: roughly half of the simulated ACM surface area was below 100 nm and did not interact with light, whereas most of the observed surface area was larger than 100 nm and interacted with light (Fig. 4e).

We performed sensitivity tests that altered emitted and boundary-condition aerosol size parameters, but these did not resolve the underestimation of simulated EVR for SMPS_SUB. Ultimately, we identified two artifacts in the two-modal (ATK + ACM) representation that impede growth from nanoparticles to submicron sizes; these artifacts are described in Sect. 3.3.

https://doi.org/10.5194/egusphere-2026-1666
Preprint. Discussion started: 27 May 2026

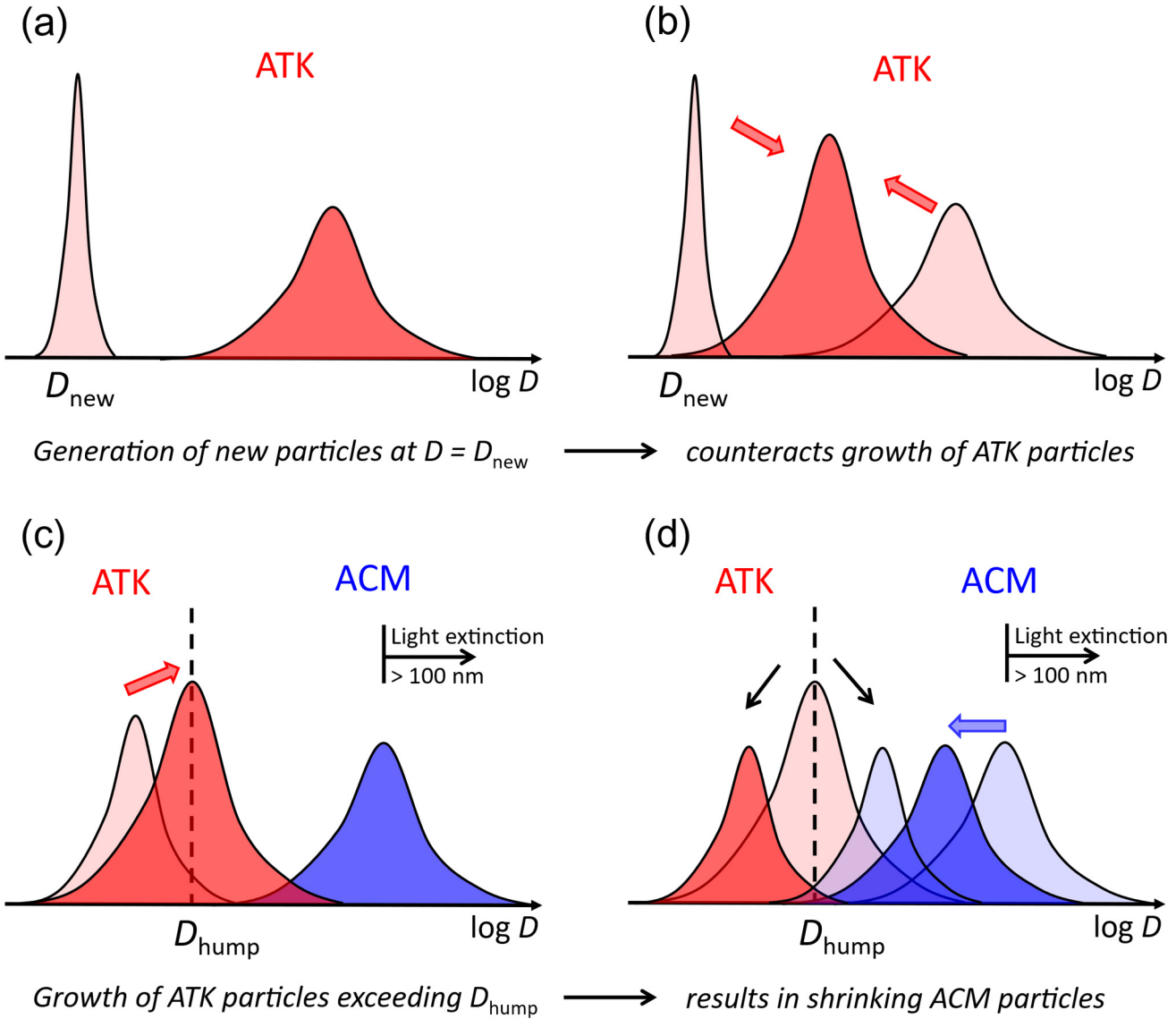

Figure 5: Conceptual illustration describing artifacts in submicron aerosol growth by two modal representations, Aitken mode (ATK) and accumulation mode (ACM): (a–b) new particle formation results in shrinking ATK mode and (c–d) growth of ATK mode results in shrinking ACM mode. (a) When the formation of new particles with a diameter of D_{new} occurs in the presence of pre-existing ATK particles, (b) it forms an unrealistic size distribution by shrinking the pre-existing ATK particles. (c) When the ATK mode grows and moments exceeding the prescribed hump diameter, D_{hump} shifts to ACM in the presence of pre-existing ACM particles, (d) it forms unrealistic size distributions by shrinking the pre-existing ACM particles.

https://doi.org/10.5194/egusphere-2026-1666
Preprint. Discussion started: 27 May 2026

3.3 Implementation of Kerminen and Kulmala (2002) parameterization and sensitivity tests to determine the best new-particle diameter D_{new} and hump diameter D_{hump}.

NHM-Chem v1.0 explicitly solved new-particle formation with a time resolution of dt_{NPF} = 1 s (Kajino et al., 2012). However, as illustrated in Figs. 5a and 5b, this produced an artifact (first artifact) in the two-modal representation: as more new particles form, the size of the ATK mode can shrink. To mitigate this, the Kerminen and Kulmala (2002) parameterization was incorporated into v2.0 as follows:

$$J_{\mathrm{app}}(D_{\mathrm{new}}, t') = J(t) exp\left[\frac{\eta}{D_{\mathrm{new}}} - \frac{\eta}{D_{\mathrm{nuc}}}\right] \quad , \qquad (12)$$

where $J_{\mathrm{app}}(D_{\mathrm{new}}, t')$ is the "apparent" nucleation rate ($m^3\ s^{-1}$) producing new particles of D_{new}, which is larger than the "real" new particles D_{nuc} (defined as 1 nm in v1.0) produced by the "real" nucleation rate $J(t)$. $t' - t$ is the time required for growth from D_{nuc} to D_{new}. η is an empirical parameter that accounts for the coagulation sink and the condensational growth rate of "real" new particles (dD_{nuc}/dt).

In NHM-Chem and other modal models, when ATK particles grow by condensation and coagulation, and part of the ATK size distribution exceeds a prescribed hump diameter (D_{hump}) (also called threshold diameter or diameter of intersection), that portion of ATK is shifted to ACM. This operation is commonly called mode merging (or renaming/reallocation). In v1.0, D_{hump} was set to 40 nm in NHM-Chem v1.0 (Kajino et al., 2012; 2021), following other studies that used values in the ranges 31–78 nm (Wilson et al., 2001) and 53 nm (Easter et al., 2004). We found, however, that 40 nm is too small in our implementation because NHM-Chem defines aerosol sizes in wet diameter, whereas many other models employ dry diameter. Therefore, the second artifact illustrated in Figs. 5c and 5d—shrinking of the ACM mode as ATK grows—tends to be more prominent in NHM-Chem.

Conversely, choosing D_{new} too large in Eq. (12) can degrade prediction accuracy, and setting D_{hump} too large will inhibit the growth of ATK to ACM. To determine optimal values, we ran sensitivity tests varying D_{new} (1–9 nm) and D_{hump} (40–120 nm). We tested both dry and wet diameters for D_{hump} ($D_{hump,dry}$ consistent with other studies, and $D_{hump,wet}$ as used in v1.0). We also tested two mode-merging methods—the gradual merging approach (GMA) and the moving center approach (MCA) —and varied the time resolution for the new-particle formulation, dt_{NPF}, which can be increased above 1 s for larger D_{new} to save CPU time. In GMA, only the portions of moments of ATK exceeding D_{hump} are shifted to ACM; in MCA, all moments are shifted to ACM when the ATK peak diameter exceeds D_{hump} (Kajino et al., 2013a). To save computation time, these sensitivity simulations used half the horizontal resolution (Δx = 60 km) with the same model domain size as in Fig. 2 (100 × 70 grids) and covered half the simulation period (January–June 2016). Fig. 6 shows daily observed and simulated EVR (SMPS_SUB) for the sensitivity tests to determine NHM-Chem v2.0; statistical scores for daily and hourly simulated and observed EVR are summarized in Table 3.

Figure 6a and the first block of Table 3 show tests in which D_{new} was increased from 1 nm (v1.0) to 9 nm; model performance did not improve substantially. The same D_{new} sensitivity tests were repeated with an enhanced $D_{hump,wet}$ = 120

https://doi.org/10.5194/egusphere-2026-1666
Preprint. Discussion started: 27 May 2026

nm (Fig. 6b and second block of Table 3). Model performance did not vary strongly with D_{new}, but the larger $D_{hump,wet}$ improved correlation R and $RMSE$ while reducing $Sim./Obs.$ ratios. Because simulations with D_{new} = 9 nm were not substantially worse than smaller D_{new} and allowed larger dt_{NPF} (saving CPU), we selected D_{new} = 9 nm for v2.0. We then ran D_{new} = 9 nm simulations with different dry and wet hump diameters ($D_{hump,dry}$, $D_{hump,wet}$: 40–120 nm) (Figs. 6c–d; third and fourth blocks of Table 3). Of the six simulations, the case with $D_{hump,dry}$ = 120 nm, yielded the best performance in R, $Sim./Obs.$, and $RMSE$. We therefore define D_{hump} by dry diameter because hygroscopic growth is not a true growth process of aerosols. In Fig. 6e (fifth block of Table 3), we compared MCA and GMA for the preferred combinations (D_{new} = 9 nm with different $D_{hump,dry}$); MCA did not outperform GMA for D_{new} = 9 nm and $D_{hump,dry}$ = 120 nm. In Fig. 6f and the final block of Table 3, we tested dt_{NPF} = 1 s (required for D_{new} = 1 nm), 10 s, and 300 s (typical dt for processes such as photochemistry and deposition). The dt_{NPF} = 300 s case performed slightly worse but was not markedly different; because it reduced simulation time (15.3 h versus ~19.0 h for shorter dt_{NPF}), we adopted dt_{NPF} = 300 s for v2.0 to save CPU time.

After reducing the artificial shrinking of ACM in v2.0, the simulated M_2 size distributions of ACM and AGR matched observations more closely (Fig. 4g). However, the simulated size distributions of ATK in v2.0 still appear unrealistic: although the large overestimation of ATK number in v1.0 was partly ameliorated in v2.0, ATK number remains substantially overestimated. This likely affects CCN predictions at higher supersaturations (D_c = 36.2 and 23.3 nm for κ = 0.3 and κ = 1.12 at T = 293.15 K and S_s = 1.0%, respectively). However, further improvement may not be possible within the two-modal framework; as proposed by Kajino et al. (2013a), a sectional approach (e.g., Matsui et al., 2011; Mao et al., 2025) is likely required to resolve submicron aerosol evolution accurately.

https://doi.org/10.5194/egusphere-2026-1666
Preprint. Discussion started: 27 May 2026

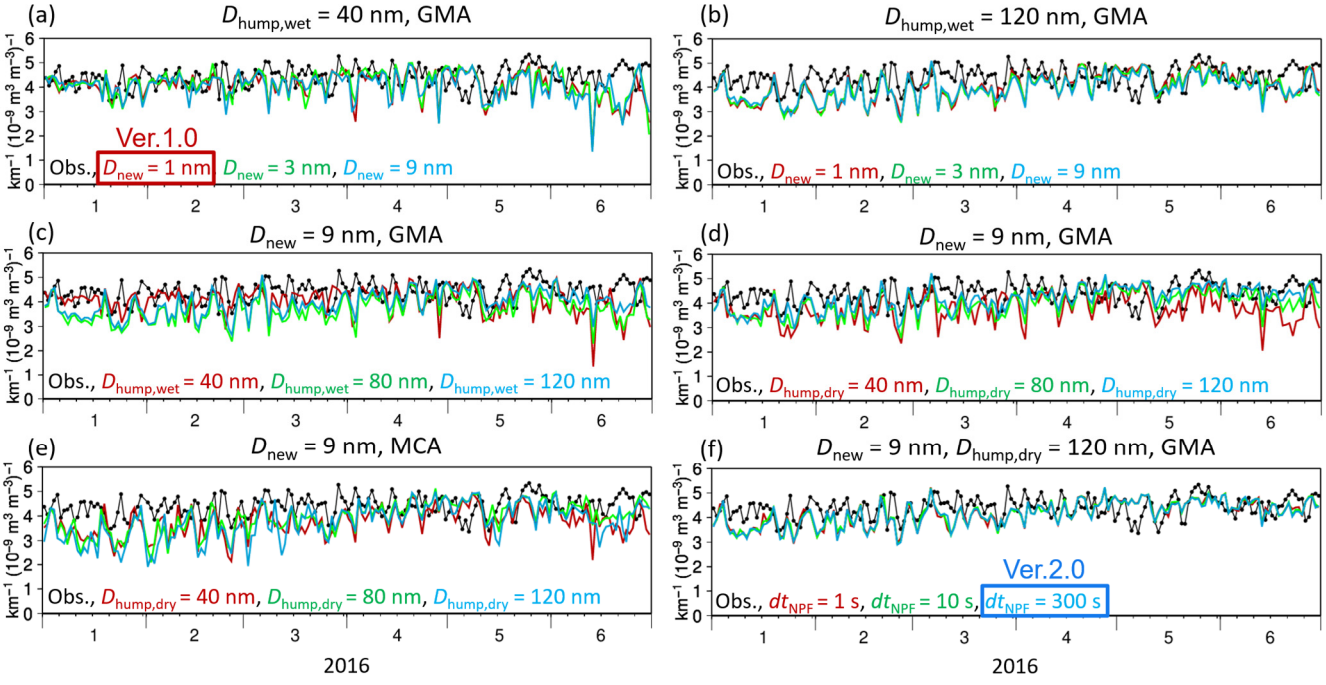

Figure 6: Time series of (black) observed and (colors) simulated daily extinction to volume ratio (EVR) from January to June 2016 for various sensitivity tests conducted by half the horizontal resolution (Δx = 60 km), regarding parameters in the two-mode representations of submicron particles, such as size of new particles D_{new}, hump diameter (when dry) $D_{hump,dry}$, hump diameter (when wet) $D_{hump,wet}$, gradual merging approach (GMA), moving center approach (MCA), and time resolution of the new particle formation calculation dt_{NPF}.

Table 3: Statistical scores comparing daily and hourly simulated and observed EVR (km^{-1} (10^{-9} m^3 m^{-3})$^{-1}$) with various sensitivity tests, as shown in Fig. 6. The six blocks from top to bottom, each encompassing three sensitivity tests, correspond to Figs. 6a to 6f.

Common setting	Sensitivity tests	*R* (daily/hourly)	*Sim./Obs.*[a] (daily/hourly)	*RMSE* (daily/hourly)	CPU time[b]
$D_{hump,wet}$ = 40 nm	D_{new} = 1 nm[c]	−0.18/−0.033	0.96/1.00	0.83/0.94	18.6 h
GMA	D_{new} = 3 nm	−0.14/−0.031	0.95/1.01	0.82/0.95	18.9 h
	D_{new} = 9 nm	−0.20/−0.032	0.94/0.98	0.83/0.92	18.8 h
$D_{hump,wet}$ = 120 nm	D_{new} = 1 nm	0.16/0.11	0.91/0.97	0.77/0.89	18.7 h
GMA	D_{new} = 3 nm	0.18/0.12	0.90/0.96	0.76/0.88	18.8 h
	D_{new} = 9 nm	0.17/0.12	0.90/0.94	0.75/0.85	18.8 h
D_{new} = 9 nm	$D_{hump,wet}$ = 40 nm	−0.20/−0.032	0.94/0.98	0.83/0.92	18.8 h
GMA	$D_{hump,wet}$ = 80 nm	0.073/0.063	0.83/0.90	0.95/0.99	18.8 h
	$D_{hump,wet}$ = 120 nm	0.17/0.12	0.90/0.94	0.75/0.85	18.8 h

https://doi.org/10.5194/egusphere-2026-1666
Preprint. Discussion started: 27 May 2026

D_{new} = 9 nm	$D_{hump,dry}$ = 40 nm	0.025/0.036	0.86/0.94	0.93/0.98	18.9 h
GMA	$D_{hump,dry}$ = 80 nm	0.21/0.15	0.92/0.96	0.72/0.83	18.7 h
	$D_{hump,dry}$ = 120 nm	0.31/0.20	0.95/1.00	0.60/0.79	18.9 h
D_{new} = 9 nm	$D_{hump,dry}$ = 40 nm	0.15/0.098	0.86/0.93	0.92/0.98	18.8 h
MCA	$D_{hump,dry}$ = 80 nm	0.25/0.16	0.90/0.97	0.80/0.97	19.0 h
	$D_{hump,dry}$ = 120 nm	0.25/0.14	0.87/0.95	0.97/1.13	19.3 h
D_{new} = 9 nm	dt_{NPF} = 1 s	0.31/0.20	0.95/1.00	0.60/0.79	19.0 h
$D_{hump,dry}$ = 120 nm	dt_{NPF} = 10 s	0.32/0.19	0.95/1.00	0.59/0.80	15.8 h
GMA	dt_{NPF} = 300 s[d]	0.30/0.19	0.95/1.00	0.61/0.80	15.3 h

[a]Simulated to observed median ratios. Observed median values are 4.43 and 4.27 for daily and hourly data, respectively.

[b]CPU Time to conduct half-year simulations with half the horizontal resolution with the same domain as Fig. 2 (January–June 2016, Δx = 60 km, 100 × 70 grids). The simulations were performed on Linux clusters using 56 cores equipped with Intel Xeon CPU E5-2697 v3 (28 cores, 2.6 GHz) and 131 GB RAM, running Rocky Linux 8.8 with Intel Fortran Compiler (version 2021.10.0) in combination with Intel MPI Library.

[c]NHM-Chem v1.0

[d]NHM-Chem v2.0

4 Evaluation of NHM-Chem v2.0 using independent measurement data

Figure 7 illustrates the time series of daily mean spherical and dust AOD observed by AD-Net and those simulated by NHM-Chem v1.0 and v2.0 at Tsukuba and Niigata. Statistical scores between observed and simulated hourly total, spherical, and dust AOD at AD-Net stations are listed in Table 4. For overall performance (All 15 stations; top block of Table 4), no remarkable improvements were found.

Simulated dust AOD by v1.0 was underestimated (*Sim./Obs.* = 0.74), whereas v2.0 overestimated dust AOD (*Sim./Obs.* = 1.8). It is promising, however, that simulated dust AOD near source regions (Ulaanbaatar and Sainshand) improved: *Sim./Obs.* at Ulaanbaatar increased from 0.44 (v1.0) to 1.0 (v2.0), and at Sainshand from 0.54 (v1.0) to 1.3 (v2.0). This is consistent with the April dust-transport event at the Niigata site shown in Figs. 7c and 7d: during that event, dust AOD from v2.0 agrees better with the observation than v1.0. On the other hand, v2.0 generally overestimates dust AOD during non-dust transport periods. The v2.0 overestimation of dust at Tsukuba in April may reflect exaggerated dust transport due to the model's crude horizontal resolution (Δx = 30 km). High mountain ranges between Niigata (Sea of Japan side) and Tsukuba (Pacific Ocean side) can block aerosol transport or scavenge aerosols by orographic precipitation, but the model's low resolution underestimates those mountain heights and therefore may underestimate orographic blocking and scavenging.

https://doi.org/10.5194/egusphere-2026-1666
Preprint. Discussion started: 27 May 2026

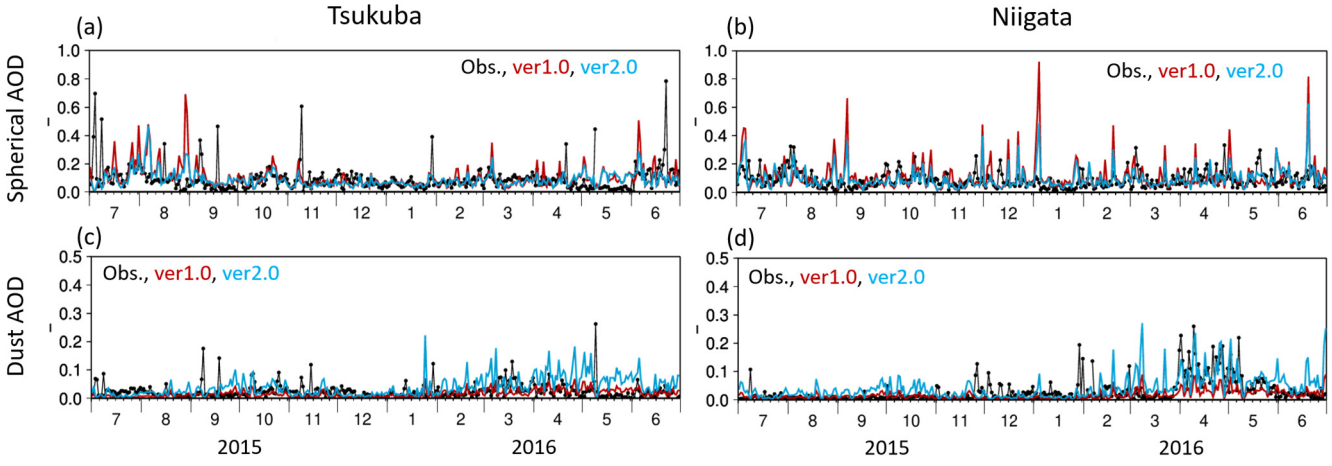

Figure 7: Time series of daily mean (black) observed and (colors) simulated (red: NHM-Chem v1.0, cyan: NHM-Chem v2.0) (a–b) aerosol optical depth (AOD) of spherical particles and (c–d) AOD of dust particles at AD-Net stations, (a, c) Tsukuba and (b, d) Niigata from July 2015 to June 2016.

https://doi.org/10.5194/egusphere-2026-1666
Preprint. Discussion started: 27 May 2026

Table 4: Statistical scores comparing hourly simulated and observed AOD (–) at all 15 AD-Net stations and eight selected stations from the upwind to the downwind of westerlies, two in Mongolia, two in Korea, and four in Japan.

Stations	Variables	*R* (v2.0/v1.0)	*Sim./Obs.* (v2.0/v1.0)	*Obs. median*	*RMSE* (v2.0/v1.0)
All 15 stations	AOD	0.20/0.15	1.1/0.88	0.11	0.15/0.18
	Spherical AOD	0.20/0.17	0.89/0.94	0.082	0.12/0.16
	Dust AOD	0.23/0.24	1.8/0.74	0.018	0.074/0.056
Ulaanbaatar	AOD	−0.075/−0.040	1.6/0.77	0.061	0.099/0.089
	Spherical AOD	−0.058/−0.022	3.2/1.8	0.016	0.057/0.042
	Dust AOD	0.025/0.021	1.0/0.44	0.037	0.071/0.071
Sainshand	AOD	0.29/0.27	1.1/0.57	0.076	0.12/0.080
	Spherical AOD	0.33/ 0.17	1.1/0.71	0.038	0.050/0.055
	Dust AOD	0.40/0.41	1.3/0.54	0.024	0.10/0.051
Seoul	AOD	0.11/0.074	0.90/0.75	0.19	0.28/0.37
	Spherical AOD	0.10/0.093	0.71/0.79	0.15	0.23/ 0.36
	Dust AOD	0.24/0.30	1.9/0.77	0.027	0.10/0.050
Jeju	AOD	0.16/0.063	1.3/1.1	0.11	0.19/0.25
	Spherical AOD	0.050/0.029	0.97/1.1	0.092	0.14/0.23
	Dust AOD	0.22/0.25	3.2/1.3	0.015	0.10/0.044
Hedo	AOD	0.029/0.023	0.81/0.85	0.15	0.15/0.16
	Spherical AOD	0.042/0.039	0.74/0.94	0.12	0.13/0.14
	Dust AOD	0.17/0.16	0.93/0.39	0.026	0.046/0.038
Matsue	AOD	0.25/0.16	0.93/0.79	0.12	0.14/0.15
	Spherical AOD	0.25/0.19	0.85/0.89	0.086	0.10/0.13
	Dust AOD	0.20/0.22	1.22/0.51	0.025	0.068/0.061
Niigata	AOD	0.15/0.065	1.3/1.2	0.082	0.16/0.19
	Spherical AOD	0.12/0.078	1.1/1.2	0.065	0.12/0.17
	Dust AOD	0.26 /0.28	3.9/1.6	0.0073	0.071/0.060
Tsukuba	AOD	0.12/0.12	1.3/1.1	0.083	0.11/0.12
	Spherical AOD	0.17/0.16	1.1/1.2	0.063	0.082/0.11
	Dust AOD	0.058/0.061	2.0/0.82	0.014	0.058/0.036

https://doi.org/10.5194/egusphere-2026-1666
Preprint. Discussion started: 27 May 2026

For spherical AOD, v2.0 generally agrees better with observations than v1.0 on statistical metrics such as *R*, *Sim./Obs.*, and *RMSE*, but the overall differences between versions are not large. This result appears inconsistent with the EVR (SMPS_SUB) analysis, which showed substantially smaller EVR in v1.0 than observed or an improvement in v2.0. It also appears inconsistent with Figs. 7a and 7b, where v2.0 mitigates v1.0's excessive peak overestimations. Several factors could cause this apparent inconsistency, and they are not easily disentangled. One possibility relates to wet-volume changes: simulated $M_{3,wet}$ by v2.0 (the denominator of EVR) is smaller than that of v1.0 (*Sim./Obs.* = 0.89 for v2.0 and 1.25 for v1.0; see Fig. A4c and Table A1). Lower condensational growth of submicron particles in v2.0 could explain the smaller $M_{3,wet}$. In v2.0, the sizes of submicron particles increased while coarse-mode particle sizes decreased, so the surface areas of submicron and coarse-mode particles changed accordingly. The relative condensation sink of gases onto submicron versus coarse-mode particles depends on the relative abundances of surface-area concentrations of the two modes; this helps explain why $M_{3,wet}$ for SMPS_SUB in v2.0, became smaller than v1.0. There is not necessarily a one-to-one correspondence between SMPS_SUB and spherical AOD, or between APS_MD and dust AOD. Spherical AOD is a column-integrated quantity to which particles of all sizes contribute, whereas SMPS measures ground-level particles smaller than ~400 nm dry diameter. Changes in the size distributions of sea-salt particles or submicron particles larger than 400 nm could substantially affect spherical AOD without being reflected in SMPS_SUB metrics. In addition, SMPS and APS are ground-based and provide near-surface measurements, whereas AOD is a columnar data; differences in vertical profiles can therefore contribute to the inconsistency.

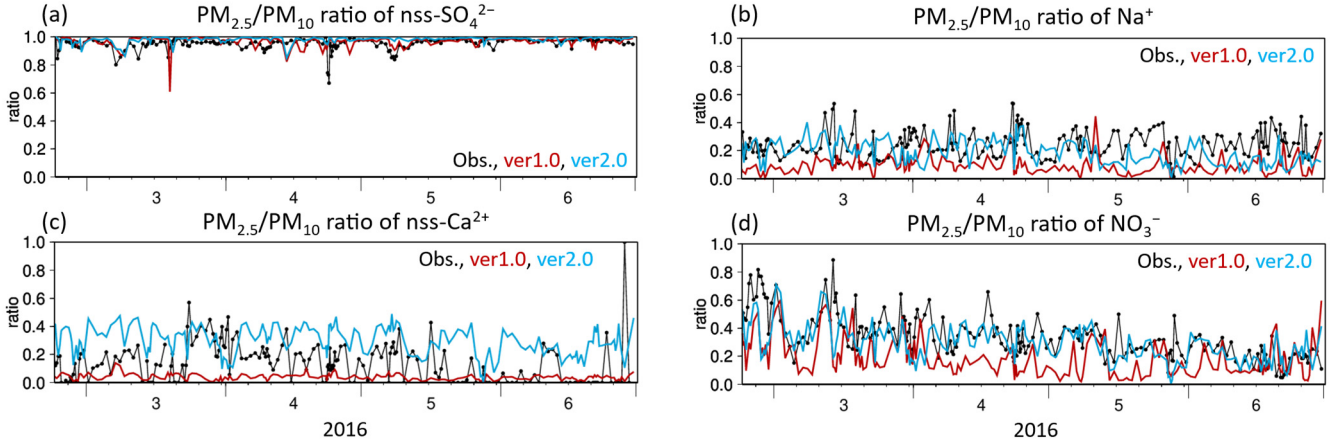

Figure 8: Time series of (black) observed and (colors) simulated (red: NHM-Chem v1.0, cyan: NHM-Chem v2.0) $PM_{2.5}/PM_{10}$ ratios of (a) nss-SO_4^{2-}, (b) Na^+, (c) nss-Ca^{2+}, and (d) NO_3^- at Tottori University from February to June 2016.

https://doi.org/10.5194/egusphere-2026-1666
Preprint. Discussion started: 27 May 2026

Time series of daily mean $PM_{2.5}/PM_{10}$ ratios of inorganic aerosol components measured at Tottori University are compared with simulations in Fig. 8. Observed median $PM_{2.5}/PM_{10}$ ratios for nss-SO_4^{2-}, Na^+, nss-Ca^{2+} (a tracer for Asian dust, largely calcite), and NO_3^- are 0.96, 0.23, 0.12, and 0.32, respectively. Simulated median $PM_{2.5}/PM_{10}$ ratios of nss-SO_4^{2-} are similar for v1.0 and v2.0 (0.98 and 0.99, respectively). Simulated median $PM_{2.5}/PM_{10}$ ratios for Na^+ and NO_3^- improved from v1.0 to v2.0: Na^+ increased from 0.081 to 0.19, and NO_3^- increased from 0.14 to 0.29. Consequently, the simulated/observed median ratios for Na^+ and NO_3^- improved from 0.35 to 0.82 and from 0.44 to 0.91, respectively. There is a well-known heterogeneous reaction between nitric acid and sodium chloride in sea-salt particles:

$$HNO_3(g) + NaCl(p) \rightarrow NaNO_3(p) + HCl(g) \quad \text{(R3)}$$

Improved sea-salt size distributions in v2.0 led to better $PM_{2.5}/PM_{10}$ ratios for Na^+ and, through the above reaction, for NO_3^-. As discussed above, changes in the relative surface-area abundance of submicron and coarse-mode particles can alter the partitioning of HNO_3 condensation between submicron and coarse-mode particles, which also affects NO_3^- $PM_{2.5}/PM_{10}$ ratios. Simulated median $PM_{2.5}/PM_{10}$ ratios for nss-Ca^{2+} were 0.038 for v1.0 and 0.30 for v2.0. The simulated/observed median ratios are 0.31 for v1.0 (underestimate) and 2.5 for v2.0 (overestimate). Nevertheless, the v2.0 $PM_{2.5}/PM_{10}$ of nss-Ca^{2+} is consistent with observations during the April Asian dust transport period, indicating an improved dust size representation in v2.0 relative to v1.0. Improved NO_3^- $PM_{2.5}/PM_{10}$ may also reflect the following heterogeneous reaction on dust (calcite):

$$2HNO_3(g) + CaCO_3(p) \rightarrow Ca(NO_3)_2(p) + H_2O(g) + CO_2(g) \quad \text{(R4)}$$

5 Comparisons of various PPVs and suggestions of the metrics of consistent aerosol model prediction, DD_{AP}

Among the PPVs proposed in Sect. 2.3, EVR was selected for intensive evaluation and model improvement. However, to demonstrate consistency and broader applicability, the model must be evaluated across multiple PPVs. A model that improves EVR but degrades other PPVs cannot be considered consistently better.

5.1 Two types of PPVs: absolute values or values relative to aerosol volumes.

Figure 9 shows the time series of daily-mean PPVs for SMPS_SUB, APS_MD, and APS_SS observed and simulated by v1.0 and v2.0. Hourly statistical scores are summarized in Table 5. To evaluate the internal consistency of simulated size distributions of aerosols, we present PPVs normalized by aerosol volume in the main text. Absolute PPVs should also be examined because the overall model predictability depends on the accuracy of absolute PPVs rather than the normalized ones. If mass concentration prediction fails, PPV absolute values will also fail even though normalized values are reasonable. Absolute PPVs are compared and evaluated in Fig. A4 and Table A1.

https://doi.org/10.5194/egusphere-2026-1666
Preprint. Discussion started: 27 May 2026

A choice arises about which aerosol volume to use for normalization: dry or wet. In this study, $M_{3,dry}$ was selected to normalize N_{tot} and N_{CCN} because aerosol number is unaffected by hygroscopic growth, and D_c is a dry diameter, respectively. By contrast, φ and β are formulated with the wet diameter of aerosols, so they were normalized by $M_{3,wet}$.

Because simulated ATK number-size distributions remain poor in both v1.0 and v2.0, the *Sim./Obs.* and *RMSE* of $N_{tot}/M_{3,dry}$ for SMPS_SUB are large (Fig. 9a; first block of Table 5). Installing the Kerminen and Kulmala (2002) parameterization in v2.0 suppressed the excessive peaks of v1.0 (Fig. 9a), lowering *RMSE.* Although *RMSE* and *R* improved in v2.0, the increase in *Sim./Obs.* indicates that not all metrics moved consistently in the same direction. By contrast, due to improved size distributions, $N_{tot}/M_{3,dry}$ performances for APS in v2.0 are generally better than v1.0 (Fig. 9b; first block of Table 5). Small differences between APS_MD and APS_SS results arise from differences in the prescribed particle densities.

https://doi.org/10.5194/egusphere-2026-1666
Preprint. Discussion started: 27 May 2026

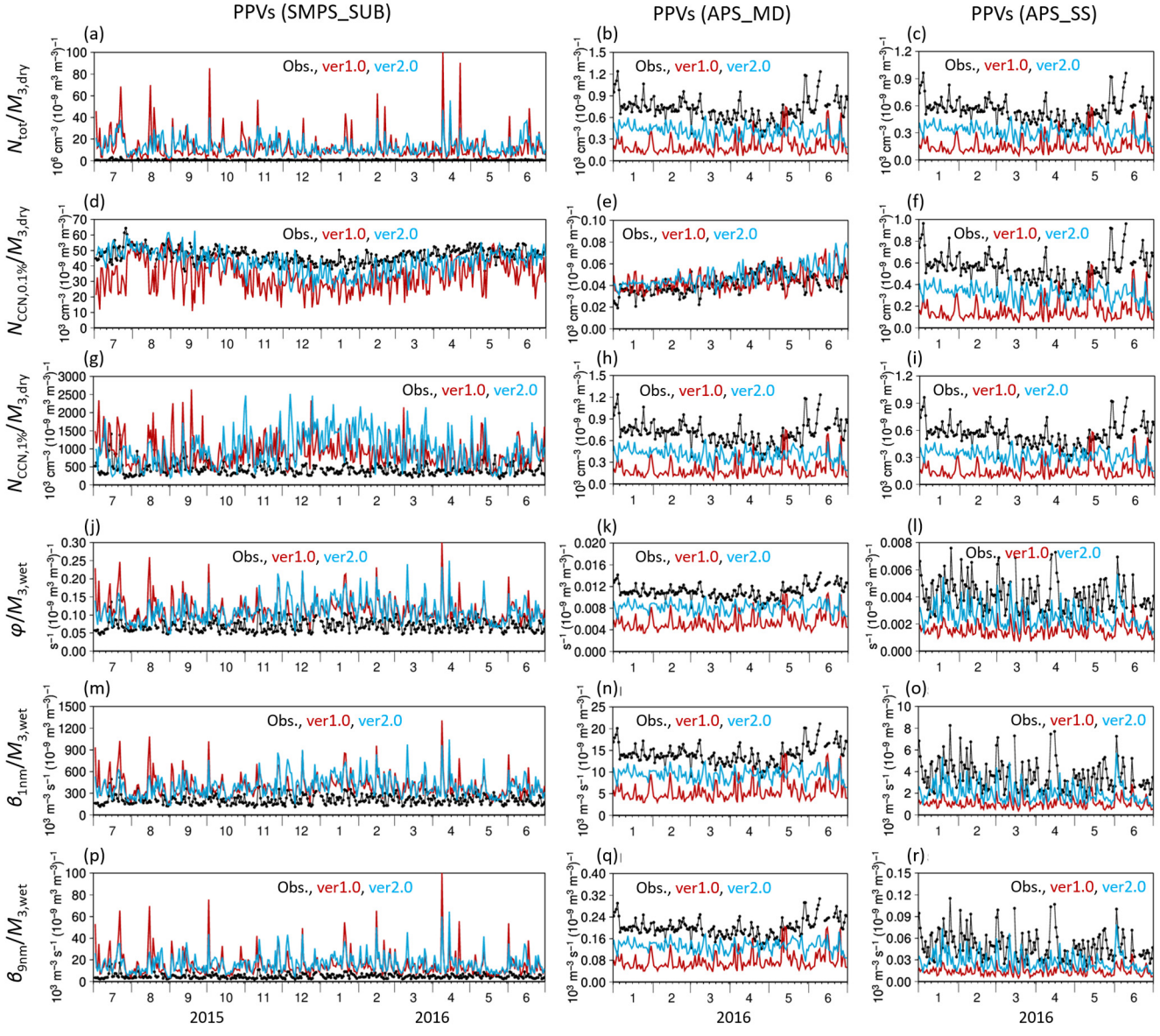

Figure 9: Daily variations of (black) observed and (colors) simulated (red: NHM-Chem v1.0, cyan: NHM-Chem v2.0) pseudo-physical variables (PPVs), (a–c) total number to dry third moment ratio ($N_{tot}/M_{3,dry}$) (Note that the unit of Y-axis for SMPS_SUB is 3 orders of magnitude larger than that of APS_MD and APS_SS), (d–f) number of CCN at supersaturation of 0.1% to dry third moment ratio ($N_{CCN,0.1\%}/M_{3,dry}$), (g–i) same as (d–f) but at supersaturation of 1% ($N_{CCN,1\%}/M_{3,dry}$), (j–l) condensational sink to wet third moment ratio ($\varphi/M_{3,wet}$), (m–o) coagulation sink of a 1 nm particle to wet third moment ratio ($\beta_{1nm}/M_{3,wet}$), and (p–r) same as (m–o) but for a particle at 9 nm diameter ($\beta_{9nm}/M_{3,wet}$), (left) for submicron particles from July 2015 to June 2016 over all SMPS size bins (SMPS_SUB), (center) for mineral dust particles from January to June 2016 (APS_MD), and (right) for sea salt particles from January to June 2016 (APS_SS).

https://doi.org/10.5194/egusphere-2026-1666
Preprint. Discussion started: 27 May 2026

N_{CCN} denotes number concentrations above the D_c. As mentioned above, for S_s = 0.1% and T = 293.15 K, D_c values are 168 nm (SUB, κ = 0.3), 1.62 µm (MD, $\kappa = 3.385\times10^{-4}$), and 108 nm (SS, κ = 1.12). For S_s = 1%, D_c values are 36.2 nm (SUB), 348 nm (MD), and 23.3 nm (SS). Because NHM-Chem reproduces larger particles more reliably, $N_{CCN,0.1\%}/M_{3,dry}$ generally performs better than $N_{CCN,\ 1\%}/M_{3,dry}$ for both model versions. The higher hygroscopicity and larger size of SS make $N_{CCN,1\%}/M_{3,dry}$ and $N_{CCN,0.1\%}/M_{3,dry}$ for APS_SS similar to $N_{tot}/M_{3,dry}$ (Figs. 9f, 9i, and 9c; first–third blocks of Table 5). Even though the hygroscopicity of MD is low, higher supersaturation (S_s = 1%) gives enough small D_c (348 nm at T = 293.15 K), so that $N_{CCN,1\%}/M_{3,dry}$ of APS_MD are the same as $N_{tot}/M_{3,dry}$ of APS_MD and $N_{CCN}/M_{3,dry}$ of APS_SS (Figs. 9h and 9b, first and third blocks of Table 5). Good performance for $N_{CCN,0.1\%}/M_{3,dry}$ of APS_MD is attributable to the consistency of simulated size distributions above 1.62 µm with observations.

$N_{CCN}/M_{3,dry}$ for SMPS_SUB, is a critical parameter for the accurate prediction of aerosol-cloud interactions. Thanks to improved submicron evolution processes in v2.0 (Sect. 3.3), $N_{CCN,0.1\%}/M_{3,dry}$ predictability is improved in warmer seasons (July–September, May–June) (Fig. 9d). However, predictability of $N_{CCN,0.1\%}/M_{3,dry}$ of both versions remain poor overall, and v2.0 performs worse than v1.0 in colder seasons (October–March) (Fig. 9g). These seasonal differences are not trivial to diagnose, but possible explanations include the following: (1) in warmer seasons, more frequent secondary formation and NPF produce larger numbers above D_c = 168 nm, improving v2.0 condensational growth representation; (2) in colder seasons, primary particles may dominate surface concentrations of aerosols, so improvements in emission of aerosol size distributions in v2.0 could explain better performance then v1.0 (Fig. 9d). Nevertheless, v2.0 still underestimates the simulated $N_{CCN,0.1\%}/M_{3,dry}$ in cold seasons and requires further refinement. Seasonal variations in the model performances of $N_{CCN,1\%}/M_{3,dry}$ (sensitive to D_c = 36.2 nm), can be linked to ATK number overestimation. The Kerminen and Kulmala parameterization in v2.0 modulates ATK evolution and reduces contamination of simulated $N_{CCN,1\%}/M_{3,dry}$ in colder seasons (see ATK size ranges ~30–40 nm in Figs. 4a and 4c). In warmer seasons, frequent NPF with D_{new} = 9 nm in v2.0 reduces ATK sizes and the contamination to $N_{CCN,1\%}/M_{3,dry}$ becomes less evident. At supersaturations above 1%, discrepancies between simulated and observed $N_{CCN}/M_{3,dry}$ should grow substantially.

https://doi.org/10.5194/egusphere-2026-1666
Preprint. Discussion started: 27 May 2026

Table 5: Statistical scores comparing hourly simulated and observed PPVs, as shown in Fig. 9.

PPVs [unit]	Measurement data and assumptions	*R* (v2.0/v1.0)	*Sim./Obs.* (v2.0/v1.0)	*Obs. median* (v2.0/v1.0)	*RMSE* (v2.0/v1.0)
$N_{tot}/M_{3,dry}$	SMPS_SUB	0.20/0.020	21/13	520	22000/26000
[10^3 cm^{-3}	APS_MD	–0.0076/0.10	0.62/0.22	0.69	0.37/0.56
(10^{-9} m^3 m^{-3})$^{-1}$)]	APS_SS	–0.0077/0.10	0.62/0.22	0.53	0.29/0.44
$N_{CCN,0.1\%}/M_{3,dry}$	SMPS_SUB	0.23/0.31	0.90/0.76	47.3	11.5/17.4
[10^3 cm^{-3}	APS_MD	0.32/0.045	1.1/1.0	0.040	0.015/0.017
(10^{-9} m^3 m^{-3})$^{-1}$]	APS_SS	–0.0077/0.10	0.62/0.22	0.53	0.29/0.44
$N_{CCN,1.0\%}/M_{3,dry}$	SMPS_SUB	–0.00016/0.11	1.8/1.8	390	860/710
[10^3 cm^{-3}	APS_MD	–0.0076/0.10	0.62/0.22	0.69	0.37/0.56
(10^{-9} m^3 m^{-3})$^{-1}$]	APS_SS	–0.0077/0.10	0.62/0.22	0.53	0.29/0.44
$\varphi/M_{3,wet}$	SMPS_SUB	0.47/0.40	1.5/1.4	0.078	0.086/0.088
[s^{-1}	APS_MD	0.032/0.026	0.77/0.45	0.011	0.0033/0.0060
(10^{-9} m^3 m^{-3})$^{-1}$]	APS_SS	0.61/0.44	0.58/0.36	0.0051	0.0024/0.0035
$\beta_{1nm}/M_{3,wet}$	SMPS_SUB	0.46/0.40	1.8/1.6	240	400/410
[10^3 m^{-3} s^{-1}	APS_MD	0.0062/0.21	0.70/0.35	14	5.5 /9.2
(10^{-9} m^3 m^{-3})$^{-1}$]	APS_SS	0.62/0.43	0.49/0.28	4.7	2.8/4.0
$B_{9nm}/M_{3,wet}$	SMPS_SUB	0.42/0.37	3.0/2.2	5.6	29/34
[10^3 m^{-3} s^{-1}	APS_MD	0.00031/0.20	0.70/0.33	0.20	0.081/0.13
(10^{-9} m^3 m^{-3})$^{-1}$]	APS_SS	0.62/0.43	0.49/0.27	0.064	0.039/0.055

For condensational growth, submicron particles are essentially in the free-molecular regime (Kajino et al., 2013a), so the mass-transport coefficient φ is proportional to surface-area concentration. As shown in Fig. 4g, the unrealistic M_2 distribution of ATK explains the overestimation of $\varphi/M_{3,wet}$ for SMPS_SUB. v2.0 shows no substantial improvement in simulated $\varphi/M_{3,wet}$ for SMPS_SUB; resolving this likely requires a sectional approach. By contrast, simulated $\varphi/M_{3,wet}$ for APS_MD and APS_SS, improved in v2.0 due to better coarse-mode size distribution parameters (Sect. 3.1; Fig. 4). Good *R* for APS_SS is aided by good correlations between simulated and observed *RH* (hence lower *R* for dry metrics such as N_{tot} and N_{CCN}). Performance trends for $\beta_{1nm}/M_{3,wet}$ and $\beta_{9nm}/M_{3,wet}$ resemble those for $\varphi/M_{3,wet}$: little change for SMPS_SUB, improvements for APS_MD and APS_SS.

Even if relative PPVs are accurately simulated, process accuracies in a 3-D framework depend on absolute PPV accuracy (volume or mass concentrations are important). Absolute PPVs, however, can be correct for the wrong reasons (for example, underpredicted relative PPV × overpredicted mass concentrations). Hence, both simulated relative and absolute PPVs (and mass concentrations) must be checked in PPVC analysis.

https://doi.org/10.5194/egusphere-2026-1666
Preprint. Discussion started: 27 May 2026

5.2 Distance of deviations between the simulated and observed aerosol physical parameters DD_{AP}

We propose a new metric for consistent prediction of aerosol microphysical parameters: DD_{AP} (distance of deviations between simulated and observed aerosol physical parameters), illustrated in Fig. 10a. A simple definition is

$$DD_{AP} = \sqrt{\sum_{k=1}^{N} \left(\widetilde{V_k^S} - \widetilde{V_k^O}\right)^2} \quad , \tag{13}$$

where N is the number of process dimensions (for example, condensation, coagulation, light extinction), and $\widetilde{V_k^S}$ and $\widetilde{V_k^O}$ are representative (normalized) simulated and observed quantities for process k. $\widetilde{V_k}$ may be a spatiotemporal average, median, fractional error, or normalized mean square error.

In this study, we define DD_{AP} as a multivariable normalized root-mean-square error composed of PPVs:

$$DD_{AP} = \sqrt{\sum_{k=1}^{N} \frac{\sum_{i=1}^{n_k}\left(s_k^i - o_k^i\right)^2}{n_k \overline{o_k}^2}} \quad , \tag{14}$$

where n_k is the number of samples for process k, s_k^i and o_k^i are simulated and observed values, and $\overline{o_k}$ is the observation mean for process k.

For the present evaluation using DD_{AP} we set N = 15, comprising EVR, $N_{CCN,0.1\%}/M_{3,dry}$, $N_{CCN,1.0\%}/M_{3,dry}$, $\varphi/M_{3,wet}$, and $\beta_{1nm}/M_{3,wet}$ for each of SMPS_SUB, APS_MD, and APS_SS. For N_{CCN}, both S_s = 0.1% and 1% are included because the sensitive size ranges are fundamentally different. For β, only D = 1 nm is included because the results of $\beta_{1nm}/M_{3,wet}$ and $\beta_{9nm}/M_{3,wet}$ are not very different. The definition is rather subjective, so different combinations of DD_{AP} can be compared. DD_{AP} shown in this study is just an example.

Figure 10b presents the DD_{AP} and NRMSE terms ($\sum_{i=1}^{n_k}\left(s_k^i - o_k^i\right)^2/n_k\overline{o_k}^2$) for each PPV. As discussed above, NHM-Chem v2.0 outperforms v1.0 in most cases—especially for coarse-mode particles—but for SMPS_SUB PPVs the two versions show similar performance (except for EVR), and v2.0 is worse for $N_{CCN,1.0\%}$ of SMPS_SUB, probably reflecting limitations of the two-modal representation. Overall, DD_{AP} values for NHM-Chem v1.0 and v2.0 are 4.2×10^{-2} and 3.5×10^{-2}, respectively, indicating that v2.0's simulated aerosol microphysics are ~17% more consistent with observations than v1.0's.

https://doi.org/10.5194/egusphere-2026-1666
Preprint. Discussion started: 27 May 2026

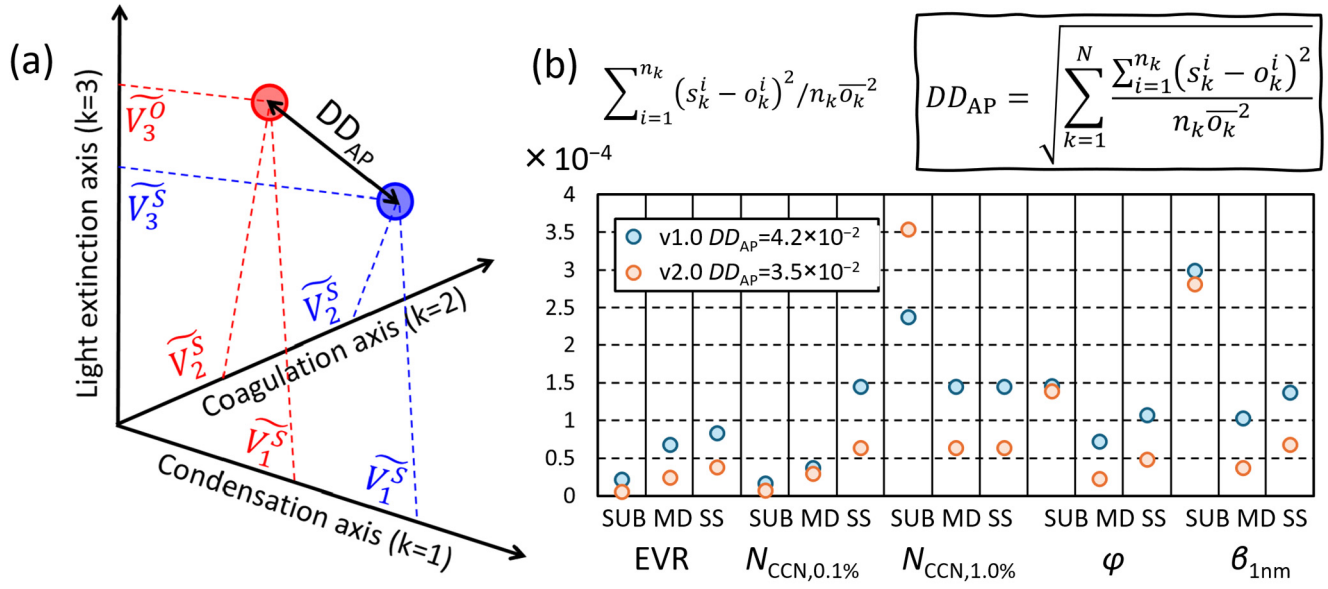

Figure 10: (a) Conceptual illustration of DD_{AP} for the case of N = 3 (condensation, coagulation, and light extinction properties). In other words, DD_{AP} is a multivariable normalized root mean square error composed of PPVs. (b) The normalized mean square error terms $\sum_{i=1}^{n_k}\left(s_k^i - o_k^i\right)^2/n_k\overline{o_k}^2$ of PPVs in the DD_{AP} equation (Eq. 14). The x-axis indicates, from left to right, SMPS_SUB, APS_MD, APS_SS of EVR, $N_{CCN,0.1\%}/M_{3,dry}$, $N_{CCN,1.0\%}/M_{3,dry}$, $\varphi/M_{3,wet}$, and $\beta_{1nm}/M_{3,wet}$.

6 Conclusions

A practical method for evaluating 3-D aerosol models using size-resolved measurements, the PPVC method, is proposed. PPVC intercompares physically meaningful variables (e.g., CCN and light-extinction coefficients) and processes (e.g., condensation rate and Brownian coagulation rate) derived from observed and simulated size distributions of aerosols together with prescribed representative parameters (e.g., hygroscopicity or refractive index). We applied PPVC to evaluate the previous model version, NHM-Chem v1.0 (Kajino et al., 2019; 2021) and the updated v2.0 (Kajino et al., 2026 and this study) using SMPS and APS data in Tsukuba. Among the PPVs we proposed, EVR was selected as the top priority for improving aerosol size-distribution predictions by NHM-Chem because EVR is central to accuracy of aerosol reanalyses and to better predictions of aerosols' direct and semi-direct climate effects. In addition to modifying emission and boundary-condition size parameters, v2.0 substantially improved EVR by (1) mitigating a critical artifact in the two-modal representation of submicron particles through implementation of the Kerminen and Kulmala (2002) parameterization (D_{new} = 9 nm) and (2) changing the hump diameter between ATK and ACM from $D_{hump,wet}$ = 40 nm to $D_{hump,dry}$ = 120 nm. Increasing D_{new} from 1 nm to 9 nm allowed dt_{NPF} to be raised from 1 s to 300 s, yielding an approximately 20% reduction in CPU time for the simulations reported here. We also propose a multivariate consistency metric, DD_{AP}. For the PPV set used here, DD_{AP}

https://doi.org/10.5194/egusphere-2026-1666
Preprint. Discussion started: 27 May 2026

values of NHM-Chem are 4.2×10^{-2} for v1.0 and 3.5×10^{-2} for v2.0, indicating that v2.0's simulated aerosol microphysical properties and processes agree better with SMPS and APS measurements at Tsukuba by roughly 17%.

The new and old model performances were evaluated by independent observation data, such as AD-Net and ion chromatography of $PM_{2.5}$ and PM_{10}. Simulated dust AOD was underestimated in v1.0 (*Sim./Obs.* = 0.74) but is overestimated in v2.0 (*Sim./Obs.* = 1.8) for the full station set. Encouragingly, v2.0 improved simulated dust AOD near source regions (for example, *Sim./Obs.* at Ulaanbaatar and Sainshand increased from 0.44/0.54 in v1.0 to 1.0/1.3 in v2.0). The v2.0 dust AOD better matches observations during a Niigata dust-transport event in April, yet tends to be overestimated during non-dust transport periods. v2.0 shows modest improvements in *R*, *Sim./Obs.*, and *RMSE* for spherical AOD, though the overall differences between versions remain small. Improvements in simulated $PM_{2.5}/PM_{10}$ ratios for Na^+ and NO_3^- are substantial: simulated/observed median ratios improved from 0.35 to 0.82 for Na^+ and from 0.44 to 0.91 for NO_3^-. These gains are attributable to better sea-salt size distributions and changes in the relative surface-area abundances of submicron versus coarse-mode particles that alter HNO_3 condensation partitioning. Remaining issues center on CCN at high supersaturations: v2.0 still overpredicts CCN at high S_s, reflecting the inherent limitations of a two-modal submicron representation. Resolving submicron evolution more likely requires sectional (bin) approaches that resolve down to ~1 nm (for example, Matsui et al., 2011; Mao et al., 2025). Such approaches increase accuracy but are computationally expensive; a promising alternative is a modal–bin hybrid model (or a triple-moment sectional model) (Kajino et al., 2013a) that aim to balance fidelity and efficiency.

A few additional practical points and limitations: APS cannot distinguish mineral dust from sea-salt, and no continuous chemical observation data were available for the whole analysis period; if nss-Ca^{2+}/Na^+ or Si/Na^+ ratios are available, dividing APS data into dust and non-dust periods would allow more targeted PPV comparisons. We did not evaluate the 0.4–1.0 μm gap between SMPS (upper limit ≈400 nm) and APS (lower limit ≈1 μm), a size range that can contain non-negligible fractions of aerosol mass and surface area. An OPC could be useful for the PPVC analysis in this size range, but most commercially available OPCs provide coarse size bins (>0.3, >0.5, >1, >2, and >5 μm), which limits PPV accuracy; high size resolution is preferable for PPVC analyses.

Not only DD_{AP} but also a similar metric can be defined and derived to evaluate cloud microphysical processes in the simulation using fog monitor and drizzle monitor data.

https://doi.org/10.5194/egusphere-2026-1666
Preprint. Discussion started: 27 May 2026

Appendix A: Additional figures and tables

This section presents additional figures and tables that serve as reference material for the main body of the manuscript.

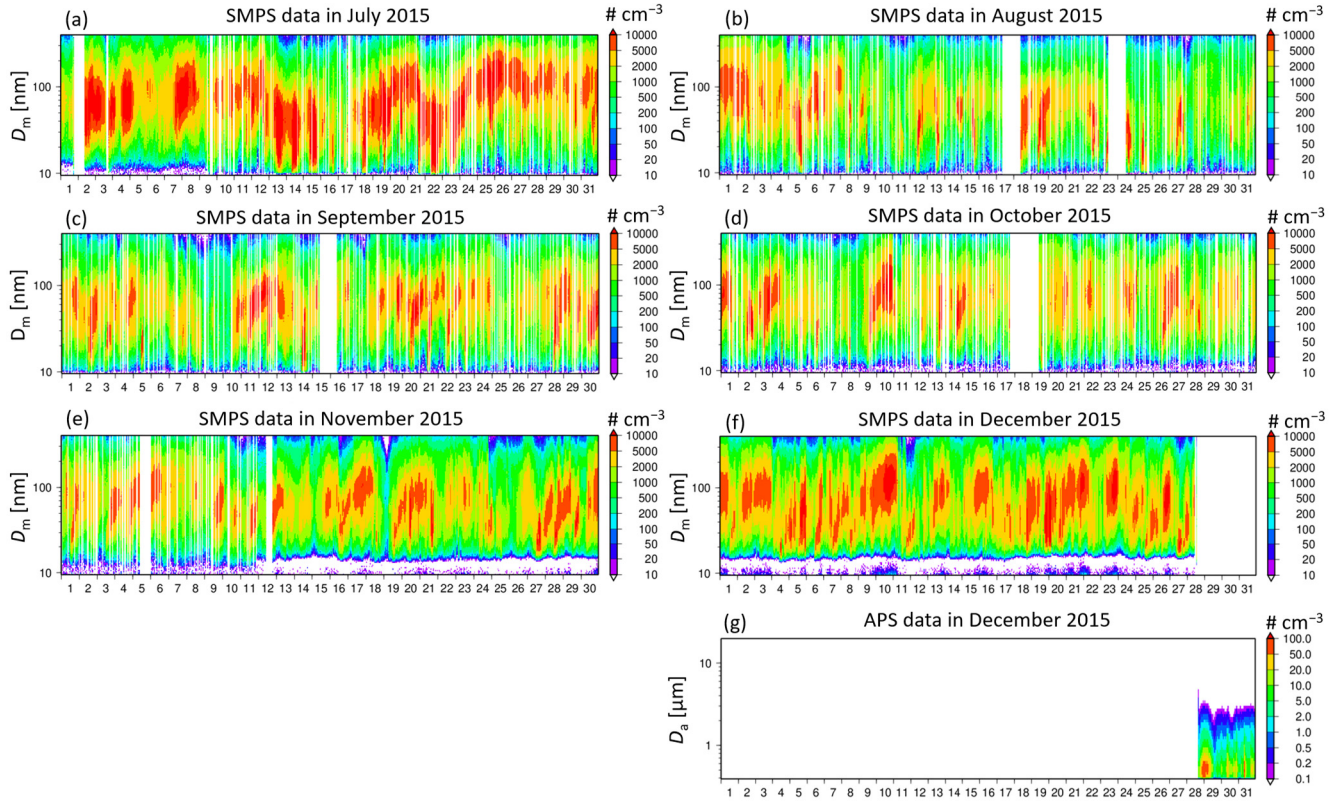

Figure A1: (a–f) Time series of hourly number size distributions of aerosols measured by SMPS at MRI for (a) July, (b) August, (c) September, (d) October, (e) November, and (f) December 2015, and (g) those measured by APS for December 2015. The y-axis indicates the mobility diameter (D_m) for SMPS and the aerodynamic diameter (D_a) for APS.

https://doi.org/10.5194/egusphere-2026-1666
Preprint. Discussion started: 27 May 2026

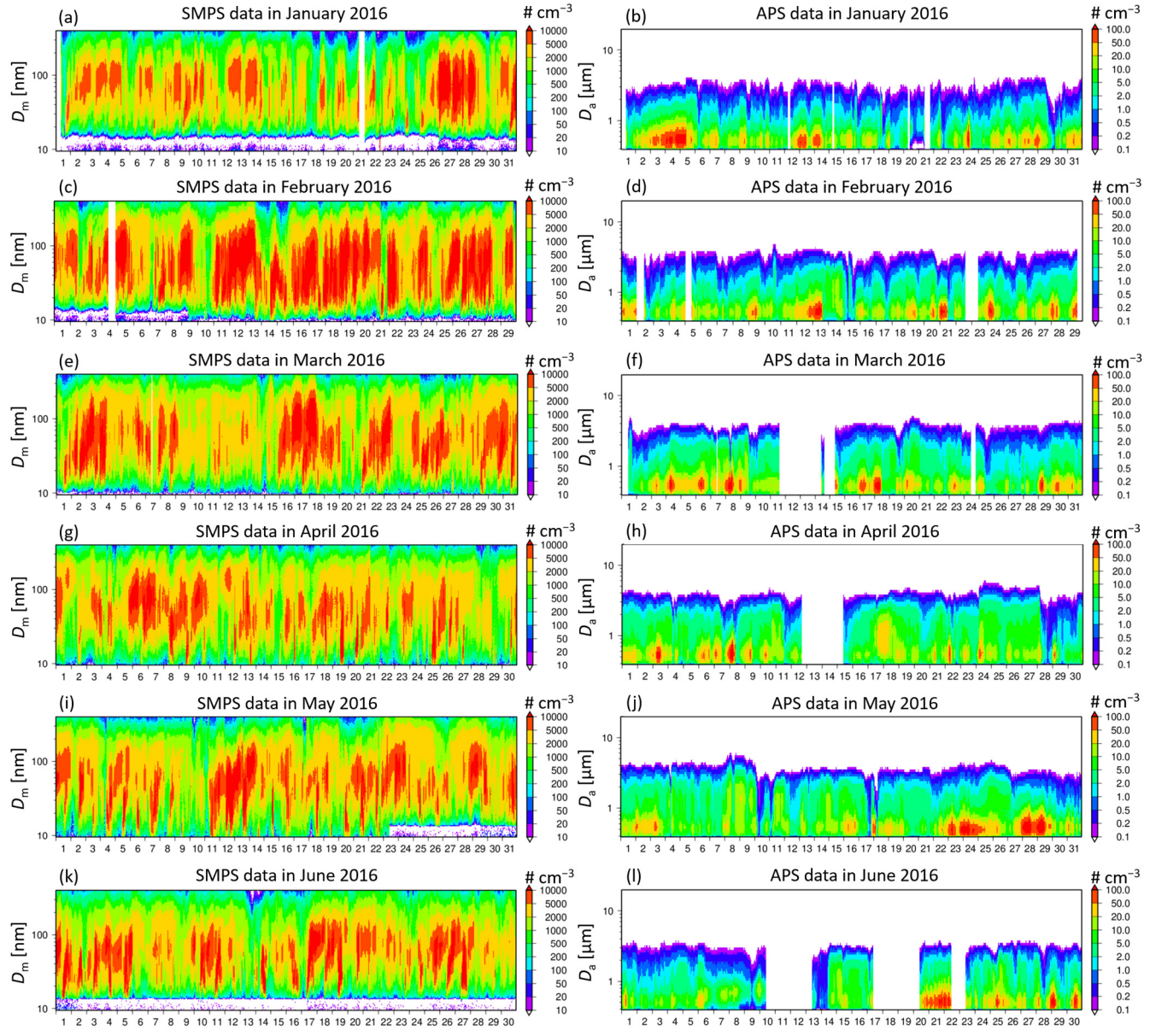

Figure A2: Time series of hourly number size distributions of aerosols measured by (left) SMPS and (right) APS for (a–b) January, (c–d) February, (e–f) March, (g–h) April, (i–j) May, and (k–l) June 2016. The y-axis indicates the mobility diameter (D_m) for SMPS and the aerodynamic diameter (D_a) for APS.

https://doi.org/10.5194/egusphere-2026-1666
Preprint. Discussion started: 27 May 2026

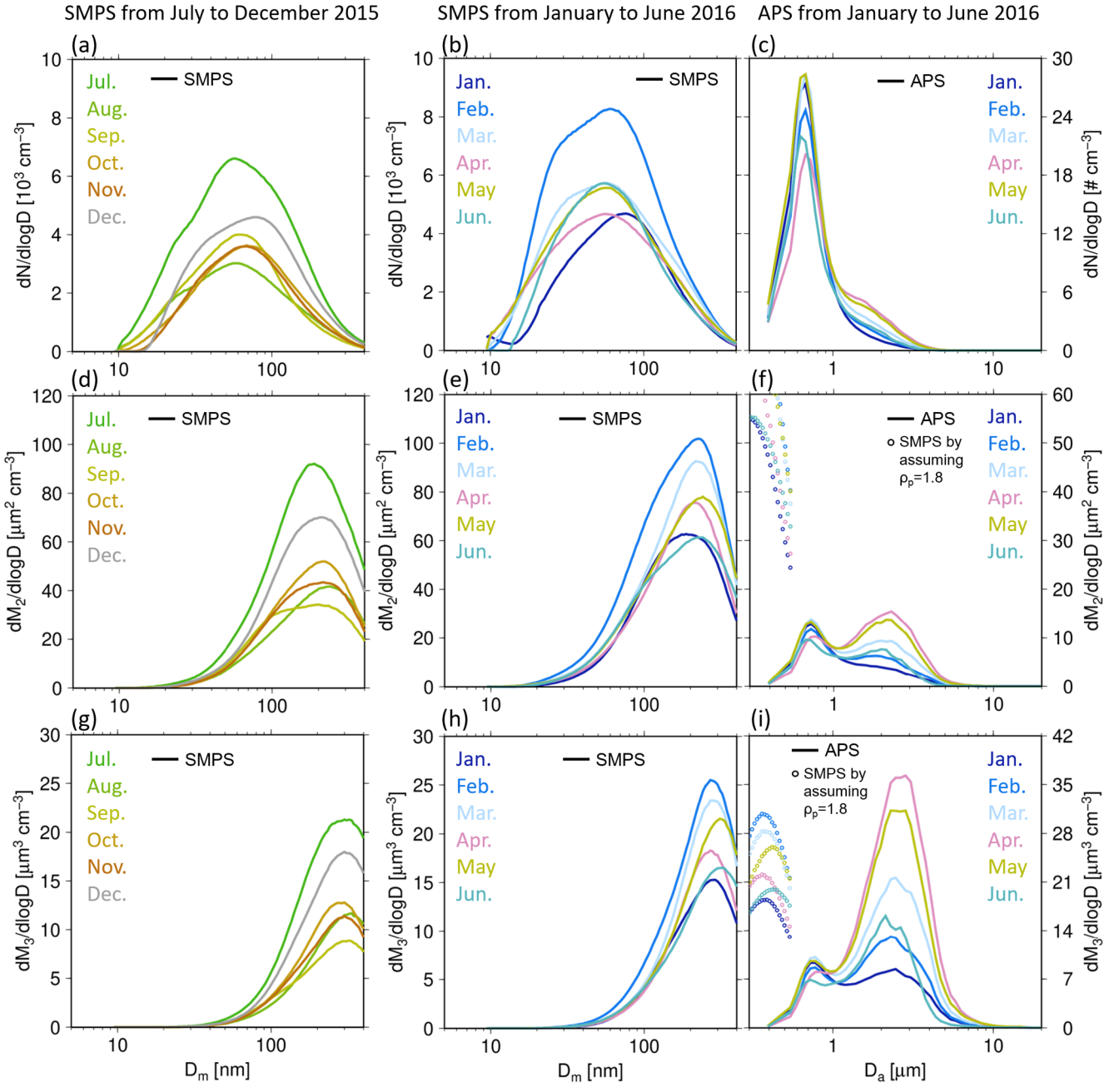

Figure A3: Monthly mean aerosol size distributions for (a–c) number (N), (d–f) second moment (M_2, proportional to surface area), and (g–i) third moment (M_3, proportional to volume): (left; a, d, and g) from July–December 2015 measured by SMPS, (center; b, e, and h) from January–June 2016 measured by SMPS, and (right; c, f, and i) from January–June 2016 measured by APS. Note that the x-axis for SMPS shows mobility diameter D_m, whereas those for APS show aerodynamic diameter D_a. In the right panels (c, f, and i), SMPS data are also depicted as open circles for reference, using the following conversion, $D_a = D_m\sqrt{\rho_p}$, where particle density $\rho_p = 1.8\times10^3$ kg m^{-3}. Note that the open circles in Fig. A3c are not shown because the converted values exceed the maximum of the y-axis.

https://doi.org/10.5194/egusphere-2026-1666
Preprint. Discussion started: 27 May 2026

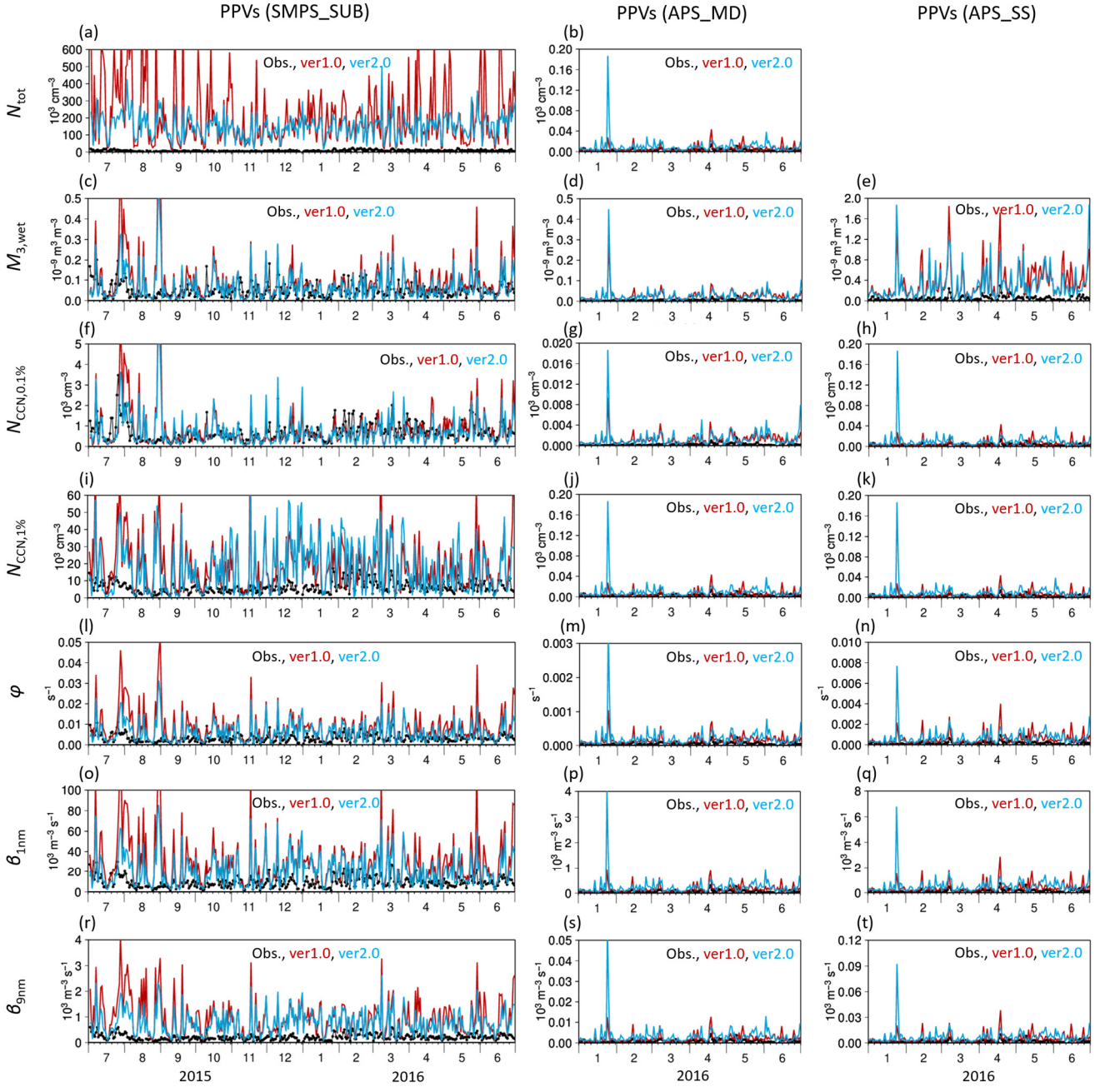

Figure A4: Daily variations of pseudo-physical variables (PPVs): observed (black) and simulated (colors; red = NHM-Chem v1.0, cyan = NHM-Chem v2.0). Panels show (a–b) total number concentrations (N_{tot}), (c–e) third moment (wet) concentrations ($M_{3,wet}$), (f–h) CCN number concentrations at supersaturation of 0.1% ($N_{CCN,0.1\%}$), (i–k) CCN number concentrations at supersaturation of 1% ($N_{CCN,1\%}$), (l–n) condensational sink (φ), (o–q) coagulation sink of a 1 nm particle (β_{1nm}), and (r–t) coagulation sink of a 9 nm particle (β_{9nm}). Panels are arranged by particle type: (left) submicron particles from July 2015–June 2016 over all SMPS size bins (SMPS_SUB), (center) mineral dust particles from January–June 2016 (APS_MD), and (right) sea-salt particles from January–June 2016 (APS_SS).

https://doi.org/10.5194/egusphere-2026-1666
Preprint. Discussion started: 27 May 2026

Table A1: Statistical scores comparing hourly simulated and observed PPVs shown in Fig. A4.

PPVs [unit]	Measurement data and assumptions	*R* (v2.0/v1.0)	*Sim./Obs.* (v2.0/v1.0)	*Obs. median* (v2.0/v1.0)	*RMSE* (v2.0/v1.0)
N_{tot} [10^3 cm^{-3}]	SMPS	0.30/0.21	17/14	3.6	100/220
	APS	0.00042/0.31	2.8/1.2	0.0013	0.017/0.0053
$M_{3,wet}$ [10^{-9} m^3 m^{-3}]	SMPS_SUB	0.31/0.31	0.89/1.25	0.015	0.059/0.080
	APS_DU	0.019/0.053	4.5/5.3	0.0019	0.043/0.031
	APS_SS	0.27/0.40	6.1/7.0	0.011	0.34/0.32
$N_{CCN,0.1\%}$ [10^3 cm^{-3}]	SMPS_SUB	0.25/0.26	0.67/0.76	0.31	0.53/0.62
	APS_DU	0.044/0.068	5.3/5.9	0.000072	0.0020/0.0011
	APS_SS	0.00042/0.31	2.8/1.2	0.0013	0.017/0.0053
$N_{CCN,1.0\%}$ [10^3 cm^{-3}]	SMPS_SUB	0.24/0.21	0.55/1.90	2.6	12/14
	APS_DU	0.00042/0.31	2.8/1.2	0.0013	0.017/0.0053
	APS_SS	0.00042/0.31	2.8/1.2	0.0013	0.017/0.0053
Φ [s^{-1}]	SMPS_SUB	0.33/0.33	1.5/2.1	0.0012	0.0040/0.0061
	APS_DU	0.020/0.20	3.3/2.4	0.00021	0.00033/0.00013
	APS_SS	0.13/0.44	3.9/2.5	0.00055	0.00081/0.00050
β_{1nm} [10^3 m^{-3} s^{-1}]	SMPS_SUB	0.32/0.32	1.9/2.4	3.7	13/20
	APS_DU	0.019/0.26	3.1/1.8	0.026	0.38/0.13
	APS_SS	0.080/0.42	3.6/2.0	0.049	0.67/0.34
B_{9nm} [10^3 m^{-3} s^{-1}]	SMPS_SUB	0.30/0.25	3.5/3.7	0.087	0.45/0.64
	APS_DU	0.018/0.27	3.1/1.7	0.00037	0.0054/0.0018
	APS_SS	0.076/0.41	3.6/1.9	0.00067	0.0091/0.0046

https://doi.org/10.5194/egusphere-2026-1666
Preprint. Discussion started: 27 May 2026

Code and data availability

The NHM-Chem v2.0 source code is not available as free and open-source software. It is available subject to a licensing agreement with the Japan Meteorological Agency (JMA). The model is available upon request for research purposes only. Access can be obtained by submitting an application including user information, research purpose, intended period of use, and contact details, along with a research plan. Requests should be directed to JMA. Use of NHM-Chem is subject to the following conditions: (i) the model is provided solely for non-commercial research purposes; (ii) redistribution of the original or modified model to third parties is not permitted; (iii) users must report research outcomes and provide any modified versions of the model to JMA, which retains the right to use them without restriction; (iv) publications and presentations based on NHM-Chem must explicitly acknowledge JMA as the mode provider; (v) JMA assumes no liability for any consequences arising from the use of the model; and (vi) the model and any modified versions must be returned to JMA upon completion of research. Detailed information on the procedures for initiating and terminating model use is available at https://www.mri-jma.go.jp/Dep/glb/nhmchem_model/application_en.html (last accessed: 31 December, 2024). The simulation results are freely available. The simulated and observed data used in the paper are available at https://doi.org/10.17632/dfk8xdbwww.1 (Kajino, 2026).

Author contributions

MK designed and conceived this study. MK developed the model together with RK, SK, TK, RI, and KY. NO conducted SMPS and APS measurements, AS, TN, and YJ conducted lidar observation, and KO conducted aerosol filter sampling and ion chromatography. MK completed the draft together with all coauthors. MK and KY acquired funding for model development and evaluation. All authors have read and agreed to the published version of the manuscript.

Competing interests

The authors declare that they have no conflict of interest.

Acknowledgments

Observations in Tottori were conducted with the assistance of Professor Y. Kurosaki of Tottori University. The authors feel obliged to Mr. Haruki Yamaguchi of JMA for his great cooperation in the development of NHM-Chem v2.0.

https://doi.org/10.5194/egusphere-2026-1666
Preprint. Discussion started: 27 May 2026

Financial support

This work was mainly supported by the Fundamental Technology Research of MRI (M5 and P4) and the Japan Society for the Promotion of Science (JSPS) KAKEHI Grant Number JP22H00562. This work was also supported by JSPS KAKENHI Grant Numbers JP23H05494 JP23K17465, JP23244095, JP17H00787, and JP15H02803, the Environment Research and Technology Development Fund of the Environmental Restoration and Conservation Agency (JPMEERF20252M03, JPMEERF20245004, JPMEERF20255M05, JPMEERF20255001, and JPMEERF20155002) funded by the Ministry of the Environment, Japan (MoEJ), and Japan Science and Technology Agency (JST) Moonshot R&D Program Grant Number JPMJMS2282-04. Observations in Tottori were partly funded by the Joint Research Program of Arid Land Research Center, Tottori University (No. 28C2011).

https://doi.org/10.5194/egusphere-2026-1666
Preprint. Discussion started: 27 May 2026

References

Andersen, S. T., Carpenter, L. J., Reed, C., Lee, J. D., Chance, R., Sherwen, T., Vaughan, A. R., Stewart, J., Edwards, P. M., Bloss, W. J., Sommariva, R., Crilley, L. R., Nott, G. J., Neves, L., Read, K., Heard, D. E., Seakins, P. W., Whalley, L. K., Boustead, G. A., Fleming, L. T., Stone, D. and Fomba, K. W.: Extensive field evidence for the release of HONO from the photolysis of nitrate aerosols, Sci. Adv., 9(3), 1–10, https://doi.org/10.1126/sciadv.add6266, 2023.

Buchard, V., Da Silva, A. M., Colarco, P. R., Darmenov, A., Randles, C. A., Govindaraju, R., Torres, O., Campbell, J. and Spurr, R.: Using the OMI aerosol index and absorption aerosol optical depth to evaluate the NASA MERRA Aerosol Reanalysis, Atmos. Chem. Phys., 15(10), 5743–5760, https://doi.org/10.5194/acp-15-5743-2015, 2015.

Burns, D. A., Lynch, J. A., Cosby, B. J., Fenn, M. E., Baron, J. S.: US EPA Clean Air Markets Div., National Acid Precipitation Assessment Program Report to Congress 2011: An integrated assessment, National Science and Technology Council, Washington, DC, 114 pp., https://obamawhitehouse.archives.gov/sites/default/files/microsites/ostp/2011_napap_508.pdf, 2011.

Cohen, A. J., Anderson, H. R., Ostro, B., Pandey, K. D., Krzyzanowski, M., Künzli, N., Gutschmidt, K., Pope, C. A., III, Romieu, I., Samet, J. M., and Smith, K. R.: Urban air pollution, in Comparative Quantification of Health Risks: Global and Regional Burden of Disease Attributable to Selected Major Risk Factors, 1st ed., edited by M. Ezzati et al., Vol. 2, pp. 1353–1453, World Health Organization, Geneva, https://doi.org/10.1175/1520-0469(1957)014%3C0115:RSORPM%3E2.0.CO;2, 2004.

Deushi, M. and Shibata, K.: Development of a Meteorological Research Institute chemistry-climate model version 2 for the study of tropospheric and stratospheric chemistry, Pap. Meteorol. Geophys., 62, 1–46, https://doi.org/10.2467/mripapers.62.1, 2011.

Easter, R. C., Ghan, S. J., Zhang, Y., Saylor, R. D., Chapman, E. G., Laulainen, N. S., Abdul-Razzak, H., Leung, L. R., Bian, X. and Zaveri, R. A.: MIRAGE: Model description and evaluation of aerosols and trace gases, J. Geophys. Res. D Atmos., 109(20), https://doi.org/10.1029/2004JD004571, 2004.

Elleman, R. A. and Covert, D. S.: Aerosol size distribution modeling with the Community Multiscale Air Quality modeling system in the Pacific Northwest: 1. Model comparison to observations, J. Geophys. Res. Atmos., 114(11), 1–16, https://doi.org/10.1029/2008JD010791, 2009.

Fast, J. D., Gustafson, W. I., Easter, R. C., Zaveri, R. A., Barnard, J. C., Chapman, E. G., Grell, G. A. and Peckham, S. E.: Evolution of ozone, particulates, and aerosol direct radiative forcing in the vicinity of Houston using a fully coupled meteorology-chemistry-aerosol model, J. Geophys. Res. Atmos., 111(21), 1–29, https://doi.org/10.1029/2005JD006721, 2006.

Flemming, J., Benedetti, A., Inness, A., Engelen J, R., Jones, L., Huijnen, V., Remy, S., Parrington, M., Suttie, M., Bozzo, A., Peuch, V. H., Akritidis, D. and Katragkou, E.: The CAMS interim Reanalysis of Carbon Monoxide, Ozone and Aerosol for 2003-2015, Atmos. Chem. Phys., 17(3), 1945–1983, https://doi.org/10.5194/acp-17-1945-2017, 2017.

https://doi.org/10.5194/egusphere-2026-1666
Preprint. Discussion started: 27 May 2026

Fuchs, N. A.: The Mechanics of Aerosols, 422 pp., *Pergamon Press*, *New York*, 1964.

Fuchs, N. A. and Sutugin, A. G.: Highly dispersed aerosols, in *Topics in Current Aerosol Research*, Vol. 2, edited by Hidy, G. M. and Brock, J. R., pp. 1–60, *Pergamon Press*, *New York*, 1971.

Gelbard, F., Tambour, Y. and Seinfeld, J. H.: Sectional representations for simulating aerosol dynamics, J. Colloid Interface Sci., 76(2), 541–556, https://doi.org/10.1016/0021-9797(80)90394-X, 1980.

Giglio, L., Randerson, J. T. and Van Der Werf, G. R.: Analysis of daily, monthly, and annual burned area using the fourth-generation global fire emissions database (GFED4), J. Geophys. Res. Biogeosciences, 118(1), 317–328, https://doi.org/10.1002/jgrg.20042, 2013.

Greenfield, S. M.: Rain scavenging of radioactive particulate matter from the atmosphere, J. Meteor., 14, 115–125, 1957.

Gregson, F. K. A., Watson, N. A., Orton, C. M., Haddrell, A. E., McCarthy, L. P., Finnie, T. J. R., Gent, N., Donaldson, G. C., Shah, P. L., Calder, J. D., Bzdek, B. R., Costello, D. and Reid, J. P.: Comparing aerosol concentrations and particle size distributions generated by singing, speaking and breathing, Aerosol Sci. Technol., 55(6), 681–691, https://doi.org/10.1080/02786826.2021.1883544, 2021.

Guenther, A., Karl, T., Harley, P., Weidinmyer, C., Palmer, P. I. and Geron, C.: Edinburgh Research Explorer Estimates of global terrestrial isoprene emissions using MEGAN (Model of Emissions of Gases and Aerosols from Nature) and Physics Estimates of global terrestrial isoprene emissions using MEGAN (Model of Emissions of Gases an, Atmos. Chem. Phys., (6), 3181–3210, https://doi.org/10.5194/acp-6-3181-2006, 2006.

Han, Z., Ueda, H., Matsuda, K., Zhang, R., Arao, K., Kanai, Y. and Hasome, H.: Model study on particle size segregation and deposition during Asian dust events in March 2002, , 109(March 2002), 1–25, https://doi.org/10.1029/2004JD004920, 2004.

Hess, M., Koepke, P. and Schult, I.: Optical Properties of Aerosols and Clouds: The Software Package OPAC, Bull. Am. Meteorol. Soc., 79(5), 831–844, https://doi.org/10.1175/1520-0477(1998)079%3C0831:OPOAAC%3E2.0.CO;2, 1998.

Inness, A., Baier, F., Benedetti, A., Bouarar, I., Chabrillat, S., Clark, H., Clerbaux, C., Coheur, P., Engelen, R. J., Errera, Q., Flemming, J., George, M., Granier, C., Hadji-Lazaro, J., Huijnen, V., Hurtmans, D., Jones, L., Kaiser, J. W., Kapsomenakis, J., Lefever, K., Leitão, J., Razinger, M., Richter, A., Schultz, M. G., Simmons, A. J., Suttie, M., Stein, O., Thépaut, J. N., Thouret, V., Vrekoussis, M. and Zerefos, C.: The MACC reanalysis: An 8 yr data set of atmospheric composition, Atmos. Chem. Phys., 13(8), 4073–4109, https://doi.org/10.5194/acp-13-4073-2013, 2013.

Ishizuka, M., Mikami, M., Tanaka, T. Y., Igarashi, Y., Kita, K., Yamada, Y., Yoshida, N., Toyoda, S., Satou, Y., Kinase, T., Ninomiya, K. and Shinohara, A.: Use of a size-resolved 1-D resuspension scheme to evaluate resuspended radioactive material associated with mineral dust particles from the ground surface, J. Environ. Radioact., 166, 436–448, https://doi.org/10.1016/j.jenvrad.2015.12.023, 2017.

Jacob, D. J.: Heterogeneous chemistry and tropospheric ozone, Atmos. Environ., 34(12–14), 2131–2159, https://doi.org/10.1016/S1352-2310(99)00462-8, 2000.

https://doi.org/10.5194/egusphere-2026-1666
Preprint. Discussion started: 27 May 2026

Jacobson, M. Z.: *Fundamentals of Atmospheric Modeling*, Second Edition, 813 pp., *Cambridge University Press*, *New York*, https://doi.org/10.1017/CBO9781139165389, 2005.

Kajino, M., Inomata, Y., Sato, K., Ueda, H., Han, Z., An, J., Katata, G., Deushi, M., Maki, T., Oshima, N., Kurokawa, J., Ohara, T., Takami, A. and Hatakeyama, S.: Development of the RAQM2 aerosol chemical transport model and predictions of the Northeast Asian aerosol mass, size, chemistry, and mixing type, Atmos. Chem. Phys., 12(24), https://doi.org/10.5194/acp-12-11833-2012, 2012.

Kajino, M., Easter, R. C. and Ghan, S. J.: Modal Bin Hybrid Model: A surface area consistent, triple-moment sectional method for use in process-oriented modeling of atmospheric aerosols, J. Geophys. Res. Atmos., 118(17), https://doi.org/10.1002/jgrd.50685, 2013a.

Kajino, M., Sato, K., Inomata, Y. and Ueda, H.: Source receptor relationships of nitrate in Northeast Asia and influence of sea salt on the long-range transport of nitrate, Atmos. Environ., 79, 67-78, https://doi.org/10.1016/j.atmosenv.2013.06.024, 2013b.

Kajino, M., Deushi, M., Sekiyama, T. T., Oshima, N., Yumimoto, K., Tanaka, T. Y., Ching, J., Hashimoto, A., Yamamoto, T., Ikegami, M., Kamada, A., Miyashita, M., Inomata, Y., Shima, S.-I., Takami, A., Shimizu, A. and Hatakeyama, S.: NHM-Chem, the Japan meteorological agency's regional meteorology – chemistry model: Model evaluations toward the consistent predictions of the chemical, physical, and optical properties of aerosols, J. Meteorol. Soc. Japan, 97(2), https://doi.org/10.2151/JMSJ.2019-020, 2019.

Kajino, M., Deushi, M., Sekiyama, T. T., Oshima, N., Yumimoto, K., Tanaka, T. Y., Ching, J., Hashimoto, A., Yamamoto, T., Ikegami, M., Kamada, A., Miyashita, M., Inomata, Y., Shima, S. I., Khatri, P., Shimizu, A., Irie, H., Adachi, K., Zaizen, Y., Igarashi, Y., Ueda, H., Maki, T. and Mikami, M.: Comparison of three aerosol representations of NHM-Chem (v1.0) for the simulations of air quality and climate-relevant variables, Geosci. Model Dev., 14(4), 2235–2264, https://doi.org/10.5194/gmd-14-2235-2021, 2021.

Kajino, M., Deushi, M., Hashimoto, A., Kudo, R., Nagasawa, R., Sekiyama, T. T., Kajikawa, T., Kayaba, S., Hara, Y., Yumimoto, K., Ganguly, D., Hayashida, S. and Maki, T.: Aerosol impacts on post-monsoon meteorology in North India predicted by the Japan Meteorological Agency's online-coupled meteorology–chemistry model NHM-Chem v2.0, Jxiv, https://doi.org/10.51094/jxiv.3338, 2026.

Kajino, M.: Simulation data from NHM-Chem v1.0 and v2.0 over Northeast Asia, used in the Pseudo-Physical Variable Comparison method, Mendeley Data, V1, https://doi.org/10.17632/dfk8xdbwww.1, 2026.

Kerminen, V. M. and Kulmala, M.: Analytical formulae connecting the "real" and the "apparent" nucleation rate and the nuclei number concentration for atmospheric nucleation events, J. Aerosol Sci., 33(4), 609–622, https://doi.org/10.1016/S0021-8502(01)00194-X, 2002.

Kobayashi, S., Ota, Y., Harada, Y., Ebita, A., Moriya, M., Onoda, H., Onogi, K., Kamahori, H., Kobayashi, C., Endo, H., Miyaoka, K. and Kiyotoshi, T.: The JRA-55 reanalysis: General specifications and basic characteristics, J. Meteorol. Soc. Japan, 93(1), 5–48, https://doi.org/10.2151/jmsj.2015-001, 2015.

https://doi.org/10.5194/egusphere-2026-1666
Preprint. Discussion started: 27 May 2026

Kurokawa, J. and Ohara, T.: Long-term historical trends in air pollutant emissions in Asia: Regional Emission inventory in ASia (REAS) version 3, Atmos. Chem. Phys., 20(21), 12761–12793, https://doi.org/10.5194/acp-20-12761-2020, 2020.

Leinonen, V., Kokkola, H., Yli-Juuti, T., Mielonen, T., Kühn, T., Nieminen, T., Heikkinen, S., Miinalainen, T., Bergman, T., Carslaw, K., Decesari, S., Fiebig, M., Hussein, T., Kivekäs, N., Krejci, R., Kulmala, M., Leskinen, A., Massling, A., Mihalopoulos, N., Mulcahy, J. P., Noe, S. M., Van Noije, T., O'connor, F. M., O'dowd, C., Olivie, D., Pernov, J. B., Petäjä, T., Seland, Ø., Schulz, M., Scott, C. E., Skov, H., Swietlicki, E., Tuch, T., Wiedensohler, A., Virtanen, A. and Mikkonen, S.: Comparison of particle number size distribution trends in ground measurements and climate models, Atmos. Chem. Phys., 22(19), 12873–12905, https://doi.org/10.5194/acp-22-12873-2022, 2022.

Li, J., Dong, H., Zeng, L., Zhang, Y., Shao, M., Wang, Z., Sun, Y. and Fu, P.: Exploring possible missing sinks of nitrate and its precursors in current air quality models-A case simulation in Pearl River delta of China using an observation-based box model, Sci. Online Lett. Atmos., 11(x), 124–128, https://doi.org/10.2151/sola.2015-029, 2015.

Li, M., Zhang, Q., Kurokawa, J., Woo, J., He, K., Lu, Z. and Ohara, T.: MIX: a mosaic Asian anthropogenic emission inventory under the international collaboration framework of the MICS-Asia and HTAP, , 935–963, https://doi.org/10.5194/acp-17-935-2017, 2017.

Luo, G. and Yu, F.: Simulation of particle formation and number concentration over the Eastern United States with the WRF-Chem + APM model, Atmos. Chem. Phys., 11(22), 11521–11533, https://doi.org/10.5194/acp-11-11521-2011, 2011.

Mann, G. W., Carslaw, K. S., Ridley, D. A., Spracklen, D. V., Pringle, K. J., Merikanto, J., Korhonen, H., Schwarz, J. P., Lee, L. A., Manktelow, P. T., Woodhouse, M. T., Schmidt, A., Breider, T. J., Emmerson, K. M., Reddington, C. L., Chipperfield, M. P. and Pickering, S. J.: Intercomparison of modal and sectional aerosol microphysics representations within the same 3-D global chemical transport model, Atmos. Chem. Phys., 12(10), 4449–4476, https://doi.org/10.5194/acp-12-4449-2012, 2012.

Mao, J., Yu, F., Murphy, B. N., An, J., Zhang, Y., Luo, G., Lin, S. and Hallar, A. G.: Improved Simulation of Particle Number Concentrations Over the US: Integrating a Size-Resolved Advanced Particle Microphysics Model Into CMAQ, J. Geophys. Res. Atmos., 130(16), https://doi.org/10.1029/2025JD044021, 2025.

Martin, S. T., Andreae, M. O., Althausen, D., Artaxo, P., Baars, H., Borrmann, S., Chen, Q., Farmer, D. K., Guenther, A., Gunthe, S. S., Jimenez, J. L., Karl, T., Longo, K., Manzi, A., Müller, T., Pauliquevis, T., Petters, M. D., Prenni, A. J., Pöschl, U., Rizzo, L. V., Schneider, J., Smith, J. N., Swietlicki, E., Tota, J., Wang, J., Wiedensohler, A. and Zorn, S. R.: An overview of the Amazonian Aerosol Characterization Experiment 2008 (AMAZE-08), Atmos. Chem. Phys., 10(23), 11415–11438, https://doi.org/10.5194/acp-10-11415-2010, 2010.

Matsui, H., Koike, M., Kondo, Y., Takegawa, N., Wiedensohler, A., Fast, J. D. and Zaveri, R. A.: Impact of new particle formation on the concentrations of aerosols and cloud condensation nuclei around Beijing, J. Geophys. Res. Atmos., 116(19), 1–19, https://doi.org/10.1029/2011JD016025, 2011.

https://doi.org/10.5194/egusphere-2026-1666
Preprint. Discussion started: 27 May 2026

Nakano, M., Kato, T., Hayashi, S., Kanada, S., Yamada, Y., and Kurihara, K.: Development of a 5-km-Mesh Cloud-System-Resolving Regional Climate Model at the Meteorological Research Institute, J. Meteorol. Soc. Jpn., 90A, 339–350, https://doi.org/10.2151/jmsj.2012-A19, 2012.

Nojiri, R., Osada, K., Kurosaki, Y., Matsuoka, M. and Sadanaga, Y.: Variations in gaseous nitric acid concentrations at Tottori, Japan: Long-range transport from the Asian continent and local production, Atmos. Environ., 274, 118988, https://doi.org/10.1016/j.atmosenv.2022.118988, 2022.

Orikasa, N., Saito, A., Yamashita, K., Tajiri, T., Zaizen, Y., Kuo, T. H., Kuo, W. C. and Murakami, M.: Seasonal Variations of Atmospheric Aerosol Particles Focused on Cloud Condensation Nuclei and Ice Nucleating Particles from Ground-Based Observations in Tsukuba, Japan, Sci. Online Lett. Atmos., 16, 212–219, https://doi.org/10.2151/sola.2020-036, 2020.

Petters, M. D. and Kreidenweis, S. M.: A single parameter representation of hygroscopic growth and cloud condensation nucleus activity Atmos. Chem. Phys., 7, 1961–1971, https://doi.org/10.5194/acp-7-1961-2007, 2007.

Petroff, A. and Zhang, L.: Development and validation of a size-resolved particle dry deposition scheme for application in aerosol transport models, Geosci. Model Dev., 3(2), 753–769, https://doi.org/10.5194/gmd-3-753-2010, 2010.

Pfeifer, S., Müller, T., Weinhold, K., Zikova, N., Dos Santos, S. M., Marinoni, A., Bischof, O. F., Kykal, C., Ries, L., Meinhardt, F., Aalto, P., Mihalopoulos, N. and Wiedensohler, A.: Intercomparison of 15 aerodynamic particle size spectrometers (APS 3321): Uncertainties in particle sizing and number size distribution, Atmos. Meas. Tech., 9(4), 1545–1551, https://doi.org/10.5194/amt-9-1545-2016, 2016.

Riemer, N., West, M., Zaveri, R. A. and Easter, R. C.: Simulating the evolution of soot mixing state with a particle-resolved aerosol model, J. Geophys. Res. Atmos., 114(9), 1–22, https://doi.org/10.1029/2008JD011073, 2009.

Rupakheti, M., Leaitch, W. R., Lohmann, U., Hayden, K., Brickell, P., Lu, G., Li, S. M., Toom-Sauntry, D., Bottenheim, J. W., Brook, J. R., Vet, R., Jayne, J. T. and Worsnop, D. R.: An intensive study of the size and composition of submicron atmospheric aerosols at a rural site in Ontario, Canada, Aerosol Sci. Technol., 39(8), 722–736, https://doi.org/10.1080/02786820500182420, 2005.

Saito, K., Fujita, T., Yamada, Y., Ishida, J., Kumagai, Y., Aranami, K., Ohmori, S., Nagasawa, R., Kumagai, S., Muroi, C., Kato, T., Eito, H., and Yamazaki, Y.: The operational JMA nonhydrostatic mesoscale model. Mon. Wea. Rev., 134, 1266-1298, https://doi.org/10.1175/MWR3120.1, 2006.

Saito, K., Ishida, J., Aranami, K., Hara, T., Segawa, T., Narita, M., and Honda, Y.: Nonhydrostatic atmospheric models operational development at JMA. J. Meteor. Soc. Japan, 85B, 271-304, https://doi.org/10.2151/jmsj.85B.271, 2007.

Shimadera, H., Hayami, H., Chatani, S., Morino, Y., Mori, Y., Morikawa, T., Yamaji, K. and Ohara, T.: Sensitivity analyses of factors influencing CMAQ performance for fine particulate nitrate, J. Air Waste Manag. Assoc., 64(4), 374–387, https://doi.org/10.1080/10962247.2013.778919, 2014.

https://doi.org/10.5194/egusphere-2026-1666
Preprint. Discussion started: 27 May 2026

Shimizu, A., Sugimoto, N., Matsui, I., Arao, K., Uno, I., Murayama, T., Kagawa, N., Aoki, K., Uchiyama, A., and Yamazaki, A.: Continuous observations of Asian dust and other aerosols by polarization lidar in China and Japan during ACE-Asia, J. Geophys. Res., 109(19), D19S17, https://doi.org/10.1029/2002JD003253, 2004.

Shimizu, A., Nishizawa, T., Jin, Y., Kim, S.-W., Wang, Z., Batdorj, D., and Sugimoto, N.: Evolution of a lidar network for tropospheric aerosol detection in East Asia, Opt. Eng., 56(3), 03219, https://doi.org/10.1117/1.OE.56.3.031219, 2016.

Spracklen, D. V., Pringle, K. J., Carslaw, K. S., Mann, G. W., Manktelow, P. and Heintzenberg, J.: Evaluation of a global aerosol microphysics model against size-resolved particle statistics in the marine atmosphere, Atmos. Chem. Phys., 7(8), 2073–2090, https://doi.org/10.5194/acp-7-2073-2007, 2007.

Sugimoto, N., Uno, I., Nishikawa, M., Shimizu, A., Matsui, I., Dong, X., Chen, Y., and Quan, H. Record heavy Asia dust in Beijing in 2002: Observations and model analysis of recent events, Geophys. Res. Lett., 30, 1640, https://doi.org/10.1029/2002GL016349, 2003.

Sugimoto, N., Matsui, I., Shimizu, A., Nishizawa, T., Hara, Y., Xie, C., Uno, I., Yumimoto, K., Wang, Z., Yoon, S.-C.: Lidar network observations of tropospheric aerosols, SPIE, 7153, https://doi.org/10.1117/12.806540, 2008.

Szopa, S., Naik, V., Adhikary, B., Artaxo, P., Berntsen, T., Collins, W. D., Aas, W., Akritidis, D., Allen, R. J., Kanaya, Y., Prather, M. J., Kuo, C., Zhai, P., Pirani, A., Connors, S., Péan, C., Berger, S., Caud, N., Chen, Y., Goldfarb, L., Gomis, M., Huang, M., Leitzell, K., Lonnoy, E., Matthews, J., Maycock, T., Waterfield, T., Yelekçi, O., Yu, R. and Zhou, B.: Short-lived Climate Forcers; Chapter 6; to the Sixth Assessment Report of the Intergovernmental Panel on Climate Change., https://doi.org/10.1017/9781009157896.008, 2021.

Tegen, I., Neubauer, D., Ferrachat, S., Drian, C. S. Le, Bey, I., Schutgens, N., Stier, P., Watson-Parris, D., Stanelle, T., Schmidt, H., Rast, S., Kokkola, H., Schultz, M., Schroeder, S., Daskalakis, N., Barthel, S., Heinold, B. and Lohmann, U.: The global aerosol-climate model ECHAM6.3-HAM2.3 -Part 1: Aerosol evaluation, Geosci. Model Dev., 12(4), 1643–1677, https://doi.org/10.5194/gmd-12-1643-2019, 2019.

Tanaka, T. Y. and Ogi, A.: Update of Japan Meteorological Agency's global mineral dust operational forecast model. Sokkou-Jihou, 84, 109-128, 2017 (in Japanese).

Wang, X., Zhang, L. and Moran, M. D.: Uncertainty assessment of current size-resolved parameterizations for below-cloud particle scavenging by rain, Atmos. Chem. Phys., 10(12), 5685–5705, https://doi.org/10.5194/acp-10-5685-2010, 2010.

Whitby, E. R., McMurry, P. H., Shankar, U., and Binkowski F. S.: Modal aerosol dynamics modeling, rep. 600/3-91/020, U. S. Environ. Prot. Agency, Research Triangle Park, N. C., https://nepis.epa.gov/Exe/ZyPURL.cgi?Dockey=30003UH4.txt, 1991.

Wilson, J., Cuvelier, C. and Raes, F.: A modeling study of global mixed aerosol fields, J. Geophys. Res. Atmos., 106(D24), 33081–33108, https://doi.org/10.1029/2000JD000198, 2001.

Yu, F. and Luo, G.: Simulation of particle size distribution with a global aerosol model: Contribution of nucleation to aerosol and CCN number concentrations, Atmos. Chem. Phys., 9(20), 7691–7710, https://doi.org/10.5194/acp-9-7691-2009, 2009.

https://doi.org/10.5194/egusphere-2026-1666
Preprint. Discussion started: 27 May 2026

Yumimoto, K., Tanaka, T. Y., Oshima, N. and Maki, T.: JRAero: the Japanese Reanalysis for Aerosol v1.0, Geosci. Model Dev., 10, 3225–3253, https://doi.org/10.5194/gmd-10-3225-2017, 2017.

Zhang, L., Wang, X., Moran, M. D. and Feng, J.: Review and uncertainty assessment of size-resolved scavenging coefficient formulations for below-cloud snow scavenging of atmospheric aerosols, Atmos. Chem. Phys., 13(19), 10005–10025, https://doi.org/10.5194/acp-13-10005-2013, 2013.